CHALMERS
UNIVERSITY OF TECHNOLOGY

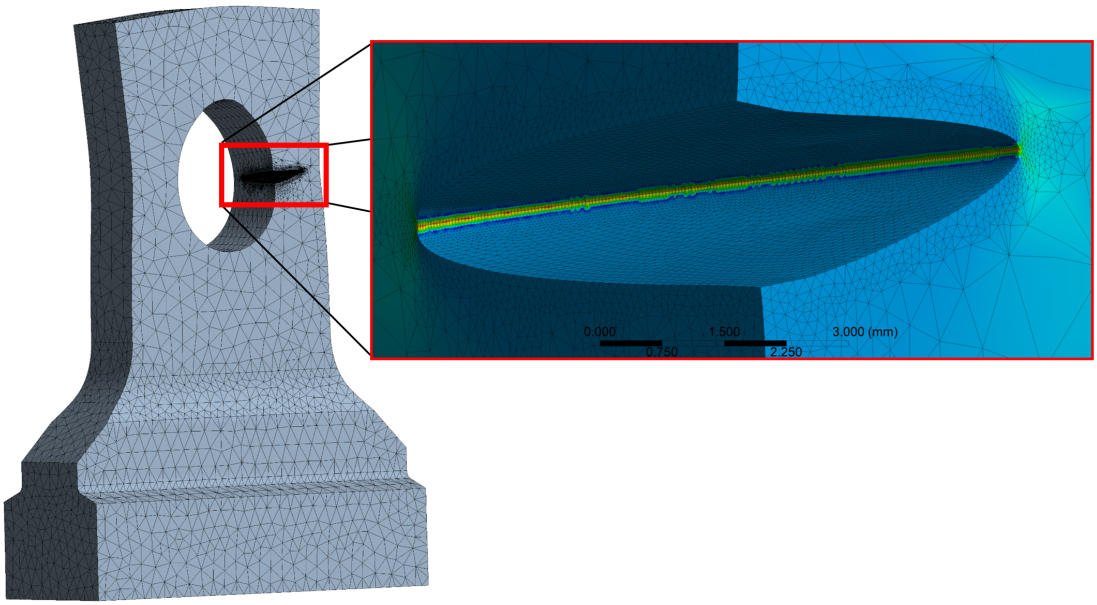

Simulation of fatigue crack growth - a comparative study

A comparison between ANSYS SMART and NASGRO with emphasis on crack-front behaviour, transition modelling, and stress ratio effects

Master's thesis in Applied Mechanics

ISAC SJÖVALL
HUGO SUNDSTRÖM

DEPARTMENT OF MECHANICS AND MARITIME SCIENCES
CHALMERS UNIVERSITY OF TECHNOLOGY
Gothenburg, Sweden 2026
www.chalmers.se

Master's thesis in Applied Mechanics

Simulation of fatigue crack growth - a comparative study

A comparison between ANSYS SMART and NASGRO with emphasis on crack-front behaviour, transition modelling, and stress ratio effects

ISAC SJÖVALL
HUGO SUNDSTRÖM

CHALMERS
UNIVERSITY OF TECHNOLOGY

Department of Mechanics and Maritime Sciences
Division of Dynamics
Chalmers University of Technology
Gothenburg, Sweden 2026

Simulation of fatigue crack growth - a comparative study
A comparison between ANSYS SMART and NASGRO with emphasis on crack-front behaviour, transition modelling, and stress ratio effects
ISAC SJÖVALL
HUGO SUNDSTRÖM

Supervisor: Sushovan Roychowdhury, GKN Aerospace Sweden AB
Examiner: Jim Brouzoulis, Department of Mechanics and Maritime Sciences

Master's Thesis 2026
Department of Mechanics and Maritime Sciences
Division of Dynamics
Chalmers University of Technology
SE-412 96 Gothenburg
Sweden
Telephone +46 (0)31 772 1000

Cover: Normal stress contour at crack front for a pin-loaded lug in ANSYS.

Typeset in LaTeX
Printed by Chalmers Reproservice
Gothenburg, Sweden 2026

Simulation of fatigue crack growth - a comparative study
A comparison between ANSYS SMART and NASGRO with emphasis on crack-front behaviour, transition modelling, and stress ratio effects
Master's Thesis in Applied Mechanics
ISAC SJÖVALL
HUGO SUNDSTRÖM
Department of Mechanics and Maritime Sciences
Division of Dynamics
Chalmers University of Technology

Abstract

Fatigue crack growth is a critical factor in the lifetime prediction and structural integrity of aerospace components. Accurate modelling of crack propagation is therefore essential for reliable design and maintenance strategies. This thesis presents a comparative study of two widely used tools for fatigue crack growth analysis: the finite element-based software ANSYS and the semi-analytical tool NASGRO. The goal is to evaluate the strengths and the limitations of these tools in predicting fatigue crack growth and to provide recommendations for their effective use, with a focus on improving accuracy.

The results show good agreement between the tools for simple loading cases, such as tensile loading with uniform crack opening. However, significant differences were observed for more complex scenarios involving non-uniform crack-front behaviour, transition modelling, and fully reversed loading. A finite element-based approach was found to better capture variations along the crack front, while NASGRO provided more computationally efficient solutions but showed limitations related to simplified crack-front representation and predefined transition modelling.

The findings highlight that the choice of analysis tool should be guided by the complexity of the loading conditions and required level of accuracy. NASGRO is well suited for efficient analysis of standard cases, while ANSYS provides improved resolution and accuracy for complex crack configurations.

Keywords: Fatigue, crack propagation, NASGRO, ANSYS SMART, fracture mechanics, SIF, surface crack, corner crack, through crack, crack transition, stress ratio.

Acknowledgements

This thesis marks the end of our academic journey and the beginning of our first steps into the engineering industry. We would like to express our sincere gratitude to Dr. Sushovan Roychowdhury, our supervisor at GKN, for his invaluable support, guidance, and continuous engagement throughout this thesis work. His introduction to the field, along with the many discussions and his insightful feedback, has been essential in shaping both the technical direction and the quality of this study.

We would also like to thank Dr. Jim Brouzoulis, our examiner at Chalmers University of Technology, for his thoughtful and constructive feedback, which has contributed to improving the academic quality of this thesis.

Furthermore, we extend our appreciation to all colleagues at GKN for their support, helpful discussions, and for providing a welcoming and stimulating working environment throughout the course of this project.

Finally, we would like to thank our families for their encouragement and support throughout the duration of this work.

Isac Sjövall, Hugo Sundström, Gothenburg, June 2026

Nomenclature

Acronyms

FCG	Fatigue Crack Growth
FE	Finite Element
FEM	Finite Element Method
GUI	Graphical User Interface
LEFM	Linear Elastic Fracture Mechanics
NASA	National Aeronautics and Space Administration
SIF	Stress Intensity Factor
SMART	Separating Morphing and Adaptive Remeshing Technology
SSY	Small Scale Yielding
SwRI	Southwest Research Institute
XFEM	eXtended Finite Element Method

List of symbols

$a,\ c,\ c_2$	Crack dimensions
Δa	Incremental crack extension
C, n, p, q	NASGRO material constants
D	Hole diameter
da/dN	Crack growth rate
E	Young's modulus
E^*	Effective modulus (plane stress/strain)
F, F_i	Geometry-dependent correction factors
f	Crack opening function
H	Specimen height

K	Stress intensity factor
$K_a,\ K_c,\ K_{c_2}$	Stress intensity factor at crack nodes $a,\ c,\ c_2$
K_{crit}	Fracture toughness
K_{op}	Crack opening stress intensity factor
ΔK	Stress intensity factor range
ΔK_{eff}	Effective stress intensity factor range
ΔK_{th}	Threshold stress intensity factor range
M_i	Bending moment components
N	Number of load cycles
ΔN	Incremental number of load cycles
P	Applied pin-loading
R	Stress ratio
S_i	Nominal stress components
t	Specimen thickness
T	Temperature
W	Specimen width
α	Plane stress/strain constraint factor
β	Surface correction factor for crack growth
μ	Shear modulus
ν	Poisson's ratio
σ_{ij}	Stress tensor components
σ_u	Ultimate tensile strength
σ_y	Yield strength

Contents

List of Figures

List of Tables

1
Introduction

Aircraft components are frequently subjected to repeated loading, which may cause microscopic damage in the structure [1]. These small defects can propagate even though the ultimate strength of the material is not reached during service loading. The accumulation of such damage over time can lead to the formation of a crack, which significantly reduces the component lifetime. In aircraft applications, fatigue accounts for approximately 55% of material failures [2]. This trend is expected to continue due to the ongoing use of metallic materials, despite extensive research into fatigue failure within the aviation industry [3].

Lifetime prediction and crack propagation simulations are therefore crucial for ensuring aviation safety. A common approach is to perform crack propagation calculations using simplified but efficient tools such as NASGRO, based on a predefined stress field [4]. NASGRO provides rapid crack growth simulations using a large library of predefined crack configurations. However, since the cross-sections of real components cannot always be modelled by the simplified geometric configurations available in NASGRO, the accuracy of the results may be limited. To achieve higher accuracy, a full-scale finite element method (FEM) that models the crack can be employed. For FEM-based crack propagation analyses to be accurate, a fine mesh with adaptive remeshing is required so that the elements adequately represents the crack geometry [5]. Such adaptive meshing approaches require complex algorithms and are computationally expensive.

This type of crack propagation capability is implemented in the commercial finite element software ANSYS, thereby enabling practical simulations of crack growth using FEM [6]. With increasing computational power and advances in efficient algorithms for in-situ crack propagation modelling, FEM-based approaches are becoming more accessible to design engineers, and concerns related to computational cost may gradually diminish. It is therefore of great interest to evaluate the efficiency and user-friendliness of such tools and to compare their accuracy in order to improve lifetime prediction capabilities within the aviation industry.

1.1 Background

Analyses of crack propagation are essential to ensure safety in critical components, such as aircraft engine structures [7]. In damage-tolerant design, engineers often employ fatigue crack growth rate relations, where the incremental crack extension

per load cycle is expressed as a function of the applied stress intensity factor range. Such formulations form the basis for numerical crack growth simulations used in engineering practice.

Several software packages are available for modelling crack propagation. In this thesis, a comparison is conducted between two of these tools: NASGRO and ANSYS. NASGRO is a suite of computer programs jointly developed by Southwest Research Institute (SwRI) and NASA [8]. The software is widely used for fracture and fatigue crack growth analyses, particularly within the aerospace industry. NASGRO can be used to calculate, among other variables, stress intensity factors (SIFs), crack growth life, and critical crack sizes. Different modules within the software are employed to evaluate these aspects. NASGRO is limited to cracks subjected to loading normal to the crack plane, corresponding to Mode I loading.

NASGRO calculates the SIFs based on stress fields obtained from analyses of the corresponding uncracked geometry, whereas ANSYS SMART computes the SIFs by explicitly modelling the crack within the finite element (FE) model. Both approaches rely on assumptions associated with linear elastic fracture mechanics (LEFM), such as small-scale yielding and predefined loading conditions, which may influence prediction accuracy depending on the application.

ANSYS includes built-in numerical solvers for crack propagation analysis. One such tool is ANSYS SMART [6], which enables automatic remeshing around the crack front during propagation. The SMART crack propagation module in ANSYS requires a crack growth law to be defined by the user. Several options are available, including the models proposed by Paris [9], Walker [10], and Forman [11], as well as the NASGRO equation [6]. To ensure a direct comparison, the NASGRO equation is used in both software tools, allowing conclusions to be drawn regarding best practices for predicting fatigue life in aircraft components. The NASGRO equation is an extension of Paris' law, modified to account for the three distinct crack propagation regions, the stress ratio, and crack closure effects.

Previous studies have shown that NASGRO provides good agreement with experimental fatigue life predictions for cases involving uniform crack loading [12, 13]. In their work, Elfving and Haeg [13] compared the results from in-situ FE simulations with NASGRO. However, their study employed the tool FRANC3D [14] and was limited to surface and embedded cracks. No such study has been performed using the latest capabilities of ANSYS, a commonly used FE program at GKN; neither have other types of cracks been investigated.

Elfving and Haeg [13] also reported that NASGRO is limited in its ability to capture detailed crack-front geometries compared to finite element approaches. Therefore, differences in fatigue life predictions between these tools must be further investigated to ensure accurate and efficient modelling of crack propagation in aerospace applications. This objective forms the primary focus of the present thesis.

1.2 Purpose

The aim of this thesis is to evaluate ANSYS[1] and NASGRO[2] in order to assess their applicability to different crack propagation problems and to examine the user-friendliness of each software when modelling fatigue crack growth. Furthermore, a comparison of the accuracy of the results produced by each tool is conducted. The overall objective can be divided into the following milestones:

- Evaluate the user-friendliness and computational efficiency of the SMART crack propagation module in ANSYS.
- Identify suitable modelling settings and perform crack growth calculations in NASGRO, followed by a comparison with corresponding ANSYS results.
- Formulate recommendations for best practices in fatigue crack growth simulations.
- Document and present the results to support knowledge dissemination in the field.

The thesis aims to contribute with answers to the following questions:

- Are the results obtained from the two software tools reasonable for the investigated crack configurations, and how do they compare?
- How does the user-friendliness of NASGRO and ANSYS vary for different crack cases?
- Are the software tools sufficient overall, or do they exhibit clear limitations?

1.3 Scope and limitations

The present thesis includes several limitations related to time, modelling assumptions, and software capabilities. The project time frame is limited to 20 weeks, which restricts the study to a finite number of crack configurations, geometries, and loading conditions.

The analyses assume that LEFM is applicable and are restricted to Mode I loading, as this is the primary crack loading mode supported by NASGRO in the contexts considered. The crack configurations investigated include through cracks, surface cracks, and corner cracks. Other crack types, such as embedded cracks, are therefore excluded from this comparative study.

In addition, thermal loading effects, including temperature gradients, are not included due to time constraints. The simulations are limited to stress ratios of $S_{min}/S_{max} = 0$ and $S_{min}/S_{max} = -1$, which are deemed sufficient to cover representative loading conditions and to enable meaningful comparison between the two software tools.

The fracture criterion employed in the analyses is based solely on exceeding the

[1] ANSYS version 2024 R1 and 2025 R2
[2] NASGRO SwRI version 11.10

fracture toughness of the material. No additional failure or stress-based criteria are evaluated within the scope of this work.

2

Theory

In the following sections, the theoretical background relevant to this thesis is presented. First, the fundamental concepts of fracture mechanics are introduced. This is followed by a description of how these concepts are employed in the numerical tools used in the present work.

2.1 Fracture mechanics fundamentals

Cracks are material discontinuities that may arise during manufacturing, service loading, fatigue, corrosion, or as a result of accidental damage. Depending on their geometry and location, cracks are categorized in order to simplify their modelling. The three crack types analysed in this thesis are surface cracks, corner cracks, and through cracks, illustrated in Figures 2.1(a) - 2.1(c).

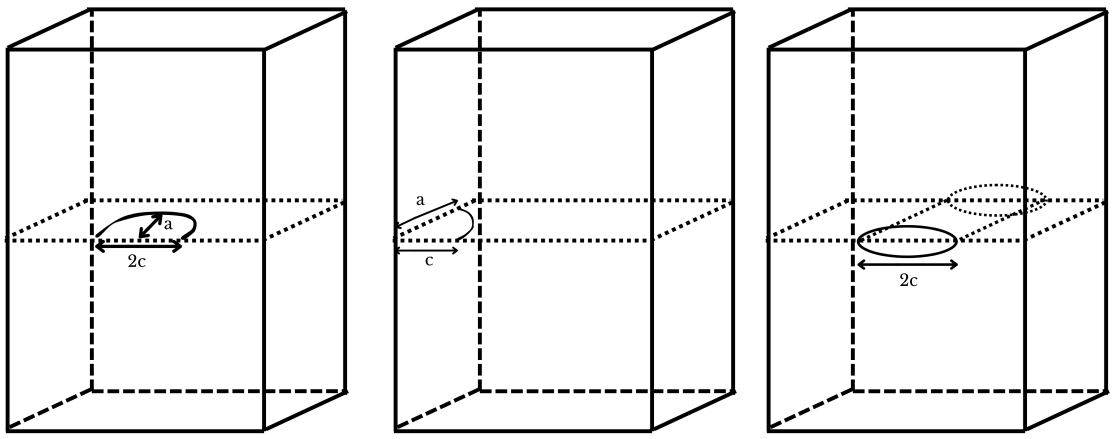

(a) **(b)** **(c)**

Figure 2.1: Illustration of **(a)** surface crack, **(b)** corner crack, and **(c)** through crack.

The cracks presented above represent idealised geometries. Crack configurations, such as cracks in more complex structures or non-symmetrical crack shapes, are also of practical relevance; however, those are not investigated in this thesis.

The theory of fracture mechanics shows that a large variety of possible cases can be

analysed by focusing on the stress state in the vicinity of the crack front [15]. The coordinate system commonly used to describe this region is illustrated in Figure 2.2. Assuming an isotropic, linear elastic material, a closed-form expression can be derived for the stress components at a point (r, θ) measured from the crack tip. This expression is given in Equation 2.1.

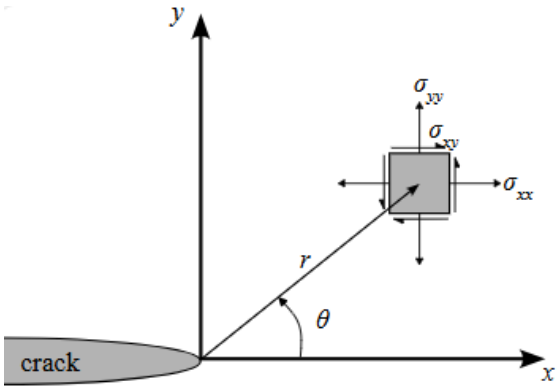

Figure 2.2: Stress field at a point (r, θ) relative to the crack front. Image taken from [16].

$$\sigma_{ij} = \left(\frac{k}{\sqrt{r}}\right) f_{ij}(\theta) + \sum_{m=0}^{\infty} A_m r^{\frac{m}{2}} g_{ij}^{(m)}(\theta) \tag{2.1}$$

Here, k is a scaling parameter, $f_{ij}(\theta)$ is a dimensionless angular function, and for the higher-order terms, A_m represents the amplitude of the mth term while $g_{ij}^{(m)}(\theta)$ is a dimensionless function of θ. The parameters k and f_{ij} depend on the applied crack loading mode. Depending on the direction of the applied loading, a crack may experience three fundamental modes of deformation [15], illustrated in Figure 2.3. Mode I corresponds to loading normal to the crack plane, Mode II represents in-plane shear loading, and Mode III corresponds to out-of-plane shear loading.

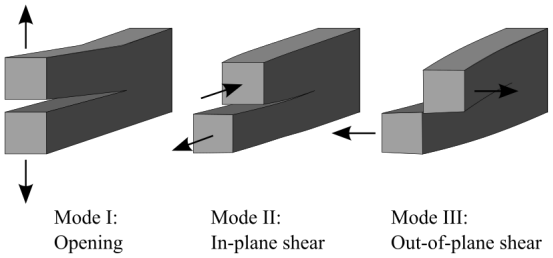

Figure 2.3: The three fundamental crack loading modes. Image taken from [17].

In Equation 2.1, it is convenient to replace the parameter k with the stress intensity factor $K = k\sqrt{2\pi}$, which is commonly designated for the three mode-dependent components as K_I, K_{II}, and K_{III}. The SIF characterises the amplitude of the stress and displacement fields near the crack tip and is directly related to the energy release rate [15]. From Equation 2.1, it can be observed that, for locations close to

the crack tip where $r \to 0$, the first term dominates. This leads to the simplified expression called the near-tip stress field

$$\lim_{r\to 0} \sigma_{ij}^{(M)} = \frac{K_M}{\sqrt{2\pi r}} f_{ij}^{(M)}(\theta) \tag{2.2}$$

where M denotes the crack loading mode. The near-tip stress field is therefore fully characterised by the corresponding SIFs. Crack instability occurs when the stress intensity factor reaches a critical value, denoted K_{crit}, commonly referred to as the fracture toughness. The fracture toughness is a material property that must be determined experimentally.

According to Equation 2.2, the theoretical stress at the crack tip approaches infinity as $r \to 0$. In real materials, such singular stresses cannot exist. Instead, the material responds through local plastic deformation, which blunts the initially sharp crack tip and results in a finite crack-tip radius [18]. This behaviour is illustrated in Figure 2.4.

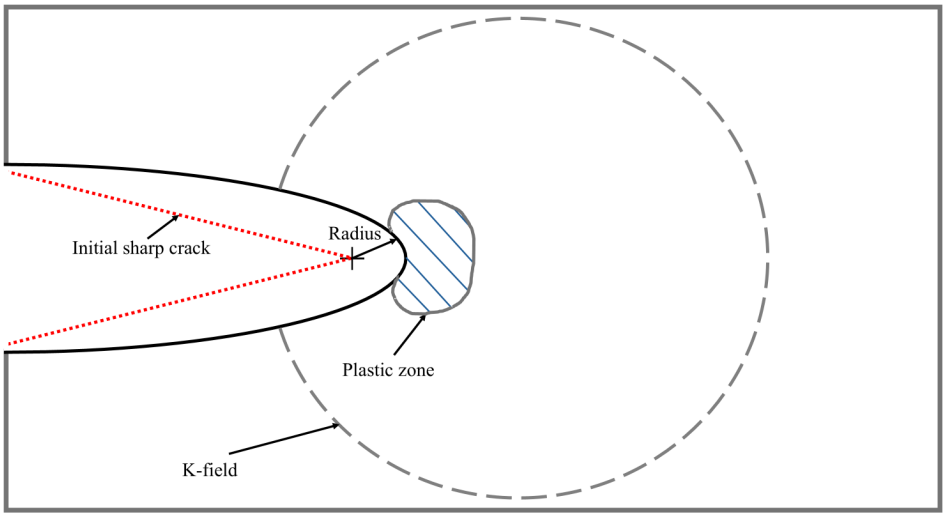

Figure 2.4: Schematic illustration of a real crack tip with a non-zero radius, including the plastic zone and surrounding K-field (not to scale).

In LEFM, it is assumed that unstable crack growth occurs when SIF due to applied loading reaches the fracture toughness K_{crit}. In this regime, fracture is considered brittle, characterised by limited plastic deformation at the structural scale [18]. In particular, LEFM assumption is valid provided that the plastic zone at the crack tip remains small compared to the region governed by the singular stress field, known as the K-field. In fracture mechanics parlance, such condition is called small-scale yielding (SSY). In this thesis, LEFM is assumed to be applicable for all analysed crack cases.

2.1.1 Surface boundary effects

For cracks embedded in an infinite body, the stress field in the vicinity of the crack front exhibits a singularity proportional to $1/\sqrt{r}$, where r is the distance from the crack front. This classical singular behaviour, however, is no longer strictly valid at locations where the crack front intersects a free surface. In such regions, the presence of the boundary modifies the local stress field. Shivakumar and Raju [19] proposed a model describing the near-field stress behaviour along a three-dimensional crack front that accounts for both interior and surface effects. According to their formulation, the stress field near the crack front can be expressed as

$$\sigma = C_0(\theta, z)r^{-1/2} + D_0(\theta, \phi)R^{\lambda_\sigma} \tag{2.3}$$

where the first term represents the classical crack-tip singularity (shown in 2.2), while the second term corresponds to an additional singular behaviour that becomes significant in the vicinity of the free surface.

The classical $1/\sqrt{r}$ singularity dominates over most of the crack front, commonly referred to as the interior region. The extent of this region depends on the material's Poisson's ratio; for example, when $\nu = 0.3$, approximately 96% of the crack front is governed by this behaviour. Near the free surface, however, a boundary layer forms in which the additional singularity becomes dominant. The thickness of this boundary layer is likewise governed by Poisson's ratio.

This model implies that while the classical singularity provides an accurate description of the stress field along the majority of the crack front, additional surface-related effects must be considered near free surfaces. Neglecting these effects may lead to inaccuracies in SIF evaluations at crack front boundaries.

2.2 SIF calculation techniques

For a limited amount of simple crack configurations and loading conditions, the SIFs can be derived in closed form. However, for complex and realistic engineering applications, analytical solutions are generally not available. In such cases, numerical methods are required to evaluate the SIFs.

The following subsections describe the SIF calculation approaches relevant to this thesis. First, a detailed description of the SIF formulations employed in NASGRO for the crack configurations investigated, including surface, corner, and through cracks. Finally, the SIF calculation methodology implemented in ANSYS is presented, which is based on the interaction integral method used for evaluating fracture parameters in finite element models.

2.2.1 SIF calculation in NASGRO

The general formulation for the SIF calculation in NASGRO is given by [4]:

$$K = (S_0F_0 + S_1F_1 + S_2F_2 + S_3F_3 + S_4F_4)\sqrt{\pi a} \tag{2.4}$$

Here, S_i represent applied stress terms, while F_i denote geometry-dependent correction factors derived for each crack configuration.

The detailed formulations, including weight functions and integration schemes to account for the geometry and distributed load, are provided in Appendix A. The nomenclature follows the conventions used in the NASGRO crack-case library and is applied consistently throughout this thesis. The investigated cases are SC30 (semi-elliptical surface crack), CC09 (quarter-elliptical corner crack), TC45 (part-elliptical through crack), and CC19 (corner crack in a lug geometry), further described in Section 3.1.

2.2.2 SIF calculation in ANSYS

In ANSYS, SIFs are calculated using the interaction integral method [6]. The interaction integral is derived from the J-integral [20] and is defined as

$$I_0 = -\int_V q_{i,j}\left[\sigma_{kl}\epsilon^{aux}_{kl}\delta_{ij} - \sigma^{aux}_{kj}u_{k,i} - \sigma_{kj}u^{aux}_{k,i}\right]dV / \int_S \delta q_n dS \tag{2.5}$$

where q_i is the crack extension vector. The quantities σ_{ij}, ϵ_{ij}, and u_i denote the stress, strain, and displacement fields, respectively, while the superscript "aux" refers to variables belonging to the auxiliary field. If thermal strains or initial strains are present in the structure, the interaction integral may be extended and expressed as

$$I = I_0 + \frac{\int_V \left[\sigma^{aux}_{kl}\epsilon^{th}_{kl,i} - \sigma^{aux}_{kl}\epsilon^{0}_{kl,i}\right]}{\int_S \delta q_n dS} - \frac{\int_S \left[t_k u^{aux}_{k,i}\right] q_i dS}{\int_S \delta q_n dS} \tag{2.6}$$

where ϵ^{th}_{ij} and ϵ^{0}_{ij} represent the thermal and initial strains, respectively, and t_i denotes the traction acting on the crack surfaces. The interaction integral is related to the SIFs according to

$$I = \frac{2}{E^*}(K_1K_1^{aux} + K_2K_2^{aux}) + \frac{1}{\mu}K_3K_3^{aux} \tag{2.7}$$

where K_1, K_2, and K_3 are the mode I, mode II, and mode III SIFs, respectively, and K_i^{aux} denotes the corresponding auxiliary SIFs. The parameter E^* depends on Young's modulus and whether a plane stress or plane strain assumption is applied, and μ is the shear modulus. All material properties required for the evaluation are defined by the user.

The auxiliary fields correspond to the asymptotic stress and strain fields for the different crack modes and are defined in a local crack-front coordinate system. ANSYS determines this local coordinate system based on the specified crack-front nodes together with the normal direction of the crack surface or the defined crack extension direction. Depending on whether thermal or initial strains are included, Equation 2.7 is evaluated using either Equation 2.5 or Equation 2.6. How ANSYS accounts for surface boundary effects in the SIF calculation is not explicitly documented and is therefore investigated further in this thesis, see Section 3.3.3.

2.3 Crack propagation

One common approach to studying fatigue crack growth is based on empirical observations, where a relationship between the cyclic crack growth rate, $\mathrm{d}a/\mathrm{d}N$, and the SIF range, ΔK, is established through laboratory testing [18]. An example of such a relationship for a given material is illustrated in Figure 2.5.

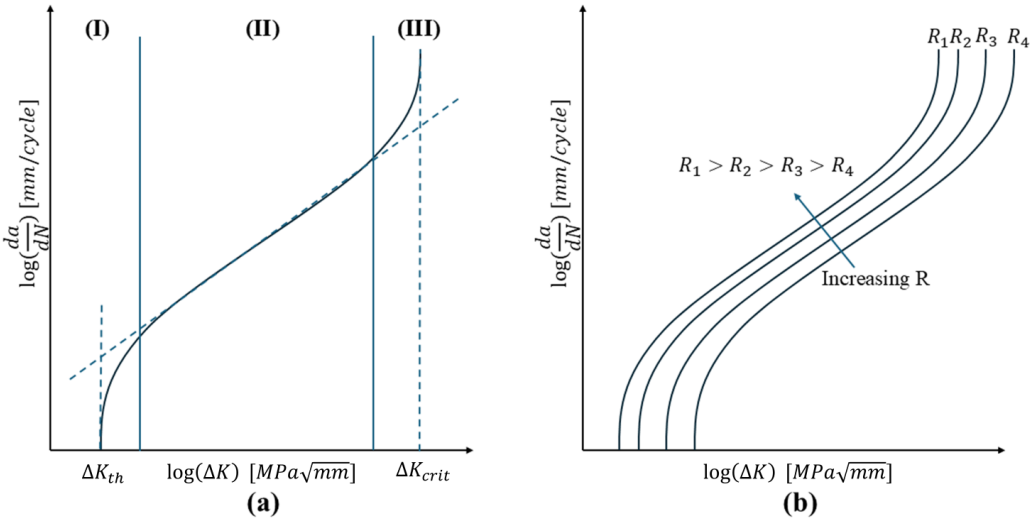

Figure 2.5: **(a):** Typical fatigue crack growth rate as a function of SIF range, illustrating the three crack growth regions. **(b):** Influence of the stress ratio R on fatigue crack growth curves.

As shown in Figure 2.5(a), the fatigue crack growth behaviour can typically be divided into three regions. Regions I and III both exhibit behaviour approaching vertical asymptotes. Region I corresponds to the threshold SIF range, where the vertical threshold indicates that no measurable crack growth occurs when $\Delta K < \Delta K_{\mathrm{th}}$ [18]. In Region III, the asymptotic behaviour corresponds to the fracture toughness, beyond which unstable crack growth occurs. In Region II, an approximately linear relationship can be observed on a log–log scale. This behaviour was described empirically by Paris [9] in the early 1960s and is expressed as

$$\frac{da}{dN} = C(\Delta K)^m \tag{2.8}$$

Equation 2.8 shows that the crack growth rate depends on the SIF range ΔK. However, to fully define a loading cycle, both the range and mean level SIFs, must be specified. As a result, ΔK alone is insufficient to describe fatigue crack growth behaviour. A stress ratio is therefore introduced as

$$R = \frac{S_{\min}}{S_{\max}} \tag{2.9}$$

where S is the gross section nominal stress and is related to the SIF through

$$K = F \cdot S\sqrt{\pi a} \tag{2.10}$$

where a is a characteristic crack dimension and F is a geometry-dependent correction factor. Combining Equations 2.9 and 2.10 yields $R = K_{\min}/K_{\max}$. The influence of the stress ratio, commonly referred to as the R-ratio, is illustrated in Figure 2.5(b). For positive stress ratios, an increase in the R-ratio generally results in a higher crack growth rate for a given nominal SIF range.

To account for the effect of mean stress Paris' law must be modified. One commonly used approach is the Walker correction [10], expressed as

$$\frac{da}{dN} = C_0 \left[\frac{\Delta K}{(1-R)^{1-\gamma}} \right]^m \tag{2.11}$$

where γ is a material constant. However, the limitations with both Paris' and Walker's forms are that they are only applicable in region II. To account for the onset of unstable crack growth in Region III, Forman [11] proposed a crack growth relation that incorporates the fracture toughness K_{crit}:

$$\frac{da}{dN} = \frac{C_2(\Delta K)^{m_2}}{(1-R)(K_{\text{crit}} - K_{\max})} \tag{2.12}$$

Another important phenomenon influencing fatigue crack growth is crack closure, which refers to the premature contact of crack faces during unloading, occurring before the minimum applied stress is reached. In the absence of crack closure, the effective stress intensity factor range is defined as ($\Delta K_{\text{eff}} = K_{\max} - K_{\min} = K_{\max}(1-R)$). However, when crack closure effects are present, the effective SIF range is more accurately described by

$$\Delta K_{\text{eff}} = \begin{cases} K_{\max} - K_{\min} & \text{if } K_{\min} > K_{\text{op}} \\ K_{\max} - K_{\text{op}} & \text{if } K_{\min} < K_{\text{op}} \end{cases} \tag{2.13}$$

where K_{op} denotes the crack opening SIF [21].

2.3.1 The NASGRO equation

NASA, in collaboration with other organizations within the aerospace industry, developed the NASGRO fatigue crack growth equation, given in Equation 2.14 [4]. The NASGRO model has demonstrated good agreement with experimental fatigue crack growth data [22, 23] and, in this thesis, is employed in two different numerical tools for the purpose of comparative analysis.

$$\frac{da}{dN} = C \left[\left(\frac{1-f}{1-R} \Delta K \right) \right]^n \frac{\left(1 - \frac{\Delta K_{\text{th}}}{\Delta K}\right)^p}{\left(1 - \frac{K_{\max}}{K_{\text{crit}}}\right)^q} \tag{2.14}$$

The parameters C, n, p, and q are material-dependent constants obtained empirically. By incorporating both the threshold SIF range and the fracture toughness,

the NASGRO equation accounts for fatigue crack growth behaviour across all three crack growth regions, shown in Figure 2.5. In addition, the effect of mean stress through the stress ratio R is included, and crack closure effects are incorporated via the crack opening function f.

The crack opening function f, originally proposed by Newman [24], is defined as

$$f = \frac{K_{\text{op}}}{K_{\max}} = \begin{cases} \max(R, A_0 + A_1 R + A_2 R^2 + A_3 R^3) & \text{if } R \geq 0 \\ A_0 + A_1 R & \text{if } -2 \leq R < 0 \end{cases} \tag{2.15}$$

The coefficients A_i are given by

$$\begin{cases} A_0 = (0.825 - 0.34\alpha + 0.05\alpha^2) \left[\cos\left(\frac{\pi}{2} \frac{S_{\max}}{\sigma_0}\right)\right]^{1/\alpha} \\ A_1 = (0.415 - 0.071\alpha) S_{\max}/\sigma_0 \\ A_2 = 1 - A_0 - A_1 - A_3 \\ A_3 = 2A_0 + A_1 - 1 \end{cases} \tag{2.16}$$

where α is the plane stress/strain constraint factor and $S_{\max}/\sigma_0$ is the ratio of the maximum applied stress to the material flow stress.

2.3.2 Numerical methods and calculations in ANSYS

ANSYS provides several numerical methods for crack propagation analysis. One such method is the Separating, Morphing, Adaptive, and Remeshing Technology (SMART), which is explained further in this section. The numerical procedures used for crack growth calculations in ANSYS SMART are also described.

2.3.2.1 ANSYS SMART

SMART is employed to simulate both static and fatigue crack growth in ANSYS [6]. In contrast to alternative crack propagation approaches, such as the eXtended Finite Element Method (XFEM), the SMART technique updates the FE mesh to reflect geometric changes in the crack as propagation occurs. This functionality is integrated directly into ANSYS SMART and allows the mesh to be updated at each user-defined increment without requiring the solver to exit or be restarted. Mesh updates are performed locally in the vicinity of the crack front and are handled automatically during the solution process.

The SMART methodology requires the finite element model to be meshed using tetrahedral elements [6]. Due to the presence of a stress singularity at the crack front, the mesh quality in this region is of particular importance. Variations in element size and shape around the crack front can significantly affect the accuracy of the computed fracture parameters and, consequently, the predicted crack growth behaviour. When defining a crack, it is necessary to specify whether the analysis is static or fatigue-based. For fatigue crack growth simulations, a crack growth law must be selected. Available options include Paris' law, the Walker equation, the Forman equation, tabular fatigue laws, and the NASGRO equation. Closure effects

may also be included within these formulations. To ensure accurate crack growth predictions, external loads must be consistently mapped from the old mesh to the updated mesh whenever remshing occurs.

As the crack propagates, SMART performs automatic mesh refinement in the region surrounding the updated crack front [6]. To achieve a balance between numerical accuracy and computational robustness, SMART coarsens the mesh in the crack wake. An appropriate mesh-coarsening strategy must be selected by the user. Three mesh-coarsening options are available: conservative, moderate, and aggressive. The conservative option, which is the default stetting, applies minimal mesh coarsening and results in a relatively large number of nodes, typically offering the highest remeshing success rate. The moderate option reduces the number of nodes and elements to a greater extent while maintaining a good likelihood of successful remeshing. The aggressive option applies rapid mesh coarsening, leading to the largest reduction in model size but also the highest risk of remeshing failure, resulting in premature termination of the simulation.

SMART determines the crack increment size based on the mesh characteristics in the crack front region in order to ensure robustness and accuracy in the analysis [6]. Depending on the initial crack size and mesh resolution, achieving accurate results may require very small increment sizes. While this improves numerical accuracy, it may also lead to a large number of increments and solution steps, increasing the computational cost. Consequently, a balance between accuracy and computational efficiency must be considered. Similar considerations apply when selecting the element size within the remeshing zone, as larger elements are more computationally efficient but may introduce inaccuracies near boundaries, interfaces, voids, and holes. These parameters are quantified in the sensitivity study described in Section 3.3.1.

2.3.2.1.1 Crack growth algorithm

In a fatigue crack growth simulation using a life-cycle approach in ANSYS, the first step consists of calculating the SIFs, as described in Section 2.2.2. Subsequently, crack growth rates da/dN are evaluated at each node along the crack front [6]. These rates are determined according to the selected crack growth law, which in this thesis corresponds to the NASGRO equation, (see eq. 2.14). Accordingly, the crack growth rate is evaluated as a function of the SIF, K, the stress ratio, R, and the temperature, T.

The crack extension Δa at the node corresponding to the maximum crack growth rate $(da/dN)_{\max}$ is set equal to the user-defined maximum incremental crack extension, $da_{\max}$. The corresponding incremental number of cycles is then calculated as

$$\Delta N = \frac{da_{\max}}{(da/dN)_{\max}} \tag{2.17}$$

from which the crack extension at all other crack front nodes can be obtained as

$$\Delta a_i = (\Delta N) \left(\frac{da}{dN} \right)_i \tag{2.18}$$

From each substep, new SIFs are computed at all crack front nodes using the interaction integral formulation (see Section 2.2.2), and the procedure is repeated until a defined termination criterion is satisfied.

2.3.3 Transition of cracks

When a surface or corner crack is subjected to fatigue loading it is possible that the crack will propagate and eventually transition into a through crack before an unstable crack growth rate is reached [25]. This transition phenomenon is illustrated below in Figure 2.6 which introduces the crack geometry parameter c_2.

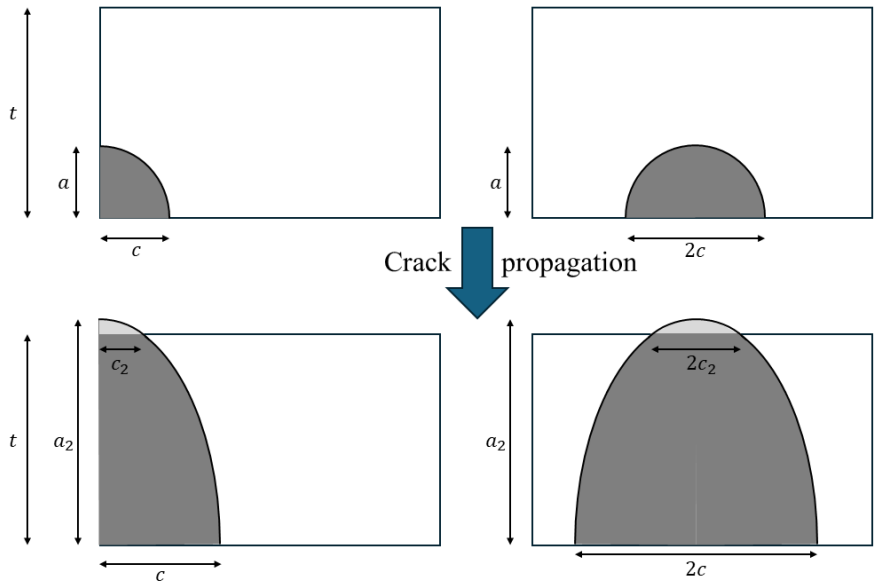

Figure 2.6: Fatigue crack growth eventually resulting in transition from corner and surface to through crack.

Several models for predicting the crack shape after transition have been proposed in literature. One such approach, presented by M. Satin et al. [25], assumes an instantaneous transition, where the front-face crack dimension c is directly transferred to the back face, such that $c_2 = c$. An alternative model assumes that the post-transition crack front adopts an elliptical shape, governed by the equation of an ellipse

$$\frac{c_2^2}{c^2} + \frac{t^2}{a_2^2} = 1 \tag{2.19}$$

which corresponds to the configurations illustrated in Figure 2.6. Experimental observations presented by M. Satin et al. indicate that the crack front after transition

exhibits a curved shape rather than a straight front. Consequently, modelling the post-transition crack front as an elliptical shape provides a more realistic representation of the observed crack growth behaviour.

Analysis of the SIFs shows that, during crack transition, the SIF at the back face increases rapidly, leading to an accelerated crack growth rate [25]. Following this stage, the SIF decreases and approaches the level of the SIF at the front face as the crack continues to propagate.

2.3.3.1 Transition model in NASGRO

In NASGRO, fatigue crack propagation is simulated using the NASGRO crack growth equation, see Equation 2.14. Crack growth continues until a predefined transition criterion is satisfied, at which point the crack geometry transitions instantaneously to a through-crack configuration. Crack propagation is then resumed using the new geometry until a critical condition is reached [4].

For surface and corner crack geometries, illustrated in Figures 2.1(a) and 2.1(b), NASGRO offers two different transition models depending on the selected post-transition crack geometry [26]. If an instantaneous transition model is selected, the crack back face assumes the same dimension as the front face, and crack propagation continues as a straight through crack, as illustrated in Figure 2.1(c). Alternatively, NASGRO allows a curved through-crack transition as illustrated in Figure 2.6. For this transition type, the back-face crack dimension is set to $c_2 = 0.2c$, after which crack growth is resumed. Crack propagation at both the front-face crack length c and the back-face crack length c_2 is then evaluated independently, resulting in a less geometrically constrained crack growth model compared to assuming uniform growth along the crack front. However, at no instance is c_2 allowed to be less than $0.2c$. This constraint is imposed so that the crack shape do not lie outside the validity range of the SIF solution utilized in NASGRO.

Two transition criteria are available in NASGRO depending on the crack type. Either the transition occurs when the crack depth satisfies $a \geq t$, corresponding to full thickness penetration, or the transition occurs when the crack depth reaches $a \geq 0.95t$.

3
Methods

This chapter presents the methodology adopted in this study. The overall approach is based on numerical simulations performed using the software packages ANSYS[1] and NASGRO[2]. The chapter first introduces the considered simulation cases, including material properties, geometries, crack configurations, and loading conditions. Thereafter, the specific simulation procedures implemented in each software are described, followed by details on model setup, parameter selection, and sensitivity analyses. Finally, the approach used for comparing and evaluating the results from the two software packages is outlined.

3.1 Simulation cases

The material used for all cases was the nickel-based superalloy Inconel 718 at room temperature. This material is widely used in the aerospace industry [2, 27] and is therefore of high practical relevance for the present study. A number of material parameters and constants are required for crack propagation analysis. The values of the most relevant material properties used in the simulations are summarized in Table 3.1. The value of C in Table 3.1 corresponds to a unit system where ΔK is expressed in MPa$\sqrt{\text{mm}}$ and crack length is expressed in mm.

Table 3.1: Material parameters of Inconel 718 at room temperature.

E	ν	σ_y	σ_u	$K_{\mathbf{crit}}$	C	n	$\Delta K_{\mathbf{th}}$
200 GPa	0.29	461.9 MPa	937.7 MPa	3475 MPa$\sqrt{\text{mm}}$	8.932×10^{-14}	3.2	83.4 MPa$\sqrt{\text{mm}}$

The crack cases investigated in this work consisted of surface cracks, corner cracks, and through cracks. These crack configurations were applied to two standard geometries: a rectangular block and a lug. Accordingly, this section is divided into two main parts corresponding to these geometries, each of which is described in terms of geometry, crack parameters, and boundary conditions.

3.1.1 Rectangular block

Examples illustrating the geometry of an initial surface crack, corner crack, and through crack are presented in Figures 2.1(a) - 2.1(c) in Section 2.1. For the rectan-

[1] ANSYS version 2024 R1 and 2025 R2
[2] NASGRO SwRI version 11.10

gular block geometry, the specific crack cases considered were, as denoted in NASGRO: SC30, CC09 and TC45. These abbreviations are used consistently throughout this work. The corresponding initial crack geometries with pertinent dimensions are shown in Figure 3.1.

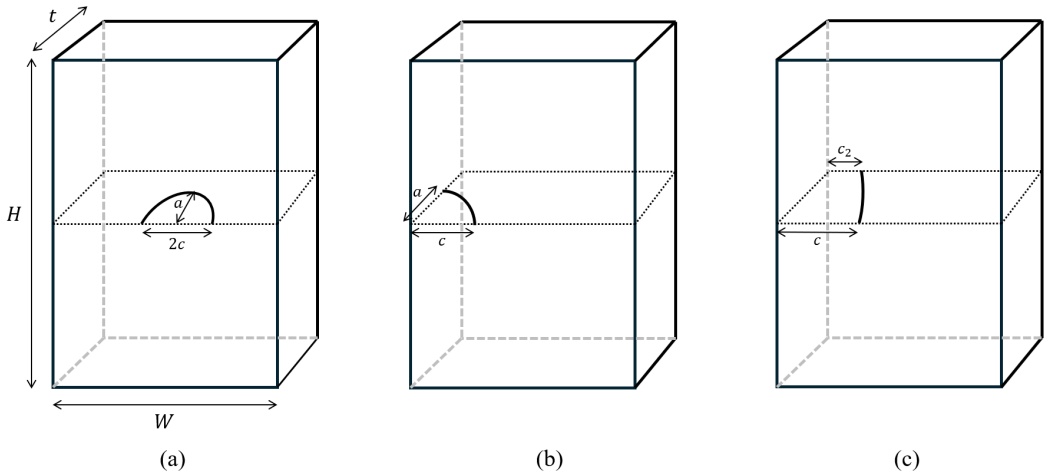

Figure 3.1: Illustration of crack configuration **(a)** SC30, **(b)** CC09, and **(c)** TC45.

3.1.1.1 Geometry, crack parameters and boundary conditions

Although the orientation and type of crack varied between cases, the underlying specimen geometry remained unchanged. The uncracked geometry consisted of a rectangular block with a height of $H = 50\,\text{mm}$, a width of $W = 20\,\text{mm}$, and a thickness of $t = 6\,\text{mm}$. The height is arbitrarily chosen since it should not affect the results in a load/stress controlled crack propagation analysis, if chosen sufficiently large. In fact, the height is not required in NASGRO analyses. The initial crack dimensions for each crack case are listed in Table 3.2.

Table 3.2: Initial crack dimensions.

Parameter	SC30	CC09	TC45
c	0.76 mm	0.76 mm	1.52 mm
a/c	1	1	N/A
c_2/c	N/A	N/A	0.5

The specimen was simulated in both software packages for a range of loading conditions and stress ratios. A schematic overview of the different loading configurations is provided in Figure 3.2.

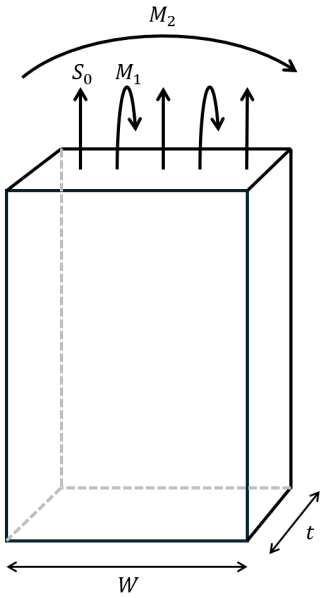

Figure 3.2: Different loads applied to the rectangular block geometry.

In this figure, the bending loads are represented by the bending moments M_1 and M_2, which are used to compute the corresponding maximum nominal stresses at the specimen edges, S_1 and S_2. These stresses are defined as:

$$S_1 = \frac{6M_1}{Wt^2}, \qquad S_2 = \frac{6M_2}{W^2t} \tag{3.1}$$

The magnitudes of the applied stress for each loading condition and crack case are summarized in Table 3.3. The SC30 crack case was not simulated under S_2 bending, as this loading configuration is not supported by NASGRO for this crack type. Furthermore, a stress magnitude of 400 MPa was applied for S_1 bending in the SC30 and TC45 cases, since a load level of 300 MPa did not result in failure governed by fracture toughness. In contrast, for a stress ratio of $R = -1$, the TC45 case was simulated using a stress magnitude of 300 MPa.

Table 3.3: Magnitude of the pressure for each simulated loading case and crack case.

Loading case	S_0	S_1	S_2
SC30	300 MPa	400 MPa	–
CC09	300 MPa	300 MPa	300 MPa
TC45	300 MPa	400 MPa	300 MPa

3.1.2 Lug

The lug was modelled with a quarter-elliptical corner crack. In NASGRO, the geometry and corresponding crack case for a quarter-elliptical corner crack emanating from a hole in a lug are represented by the case denoted as CC19. The geometries with the initial crack as implemented in both NASGRO and ANSYS are shown in Figure 3.3.

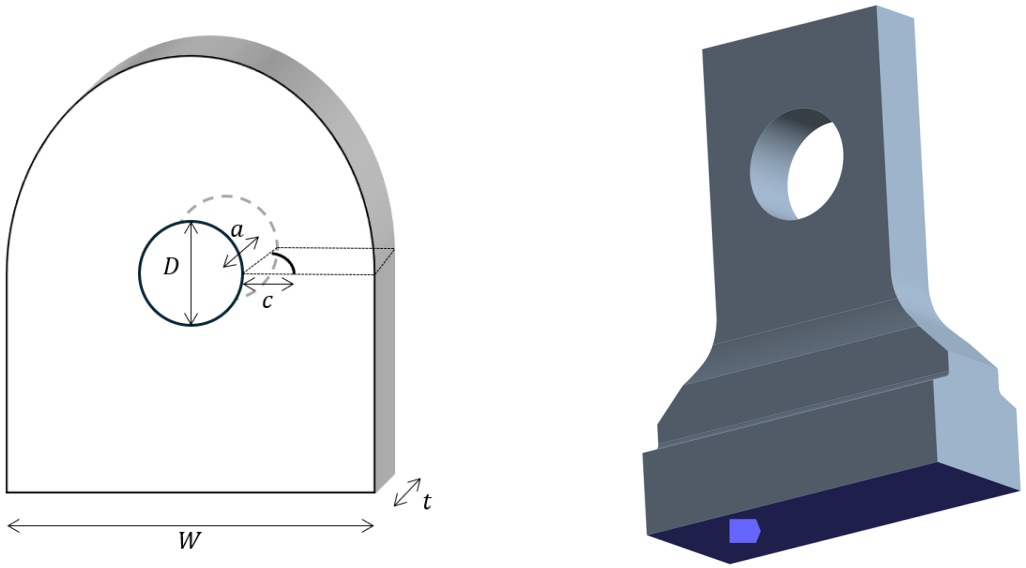

(a) **(b)**

Figure 3.3: Geometry of lug with initial crack in **(a):** NASGRO, **(b):** ANSYS. Fixed support applied at bottom edge in both figures, marked blue in **(b)**.

3.1.2.1 Geometry, crack parameters and boundary conditions

Compared to the rectangular block geometry, the lug exhibits a more complex geometry, which primarily affects the definition and implementation of the boundary conditions. The key geometric parameters defining the lug were the hole diameter $D = 16\,\text{mm}$, the thickness $t = 9\,\text{mm}$, and the width $W = 30\,\text{mm}$. The initial crack parameters were chosen to be identical to those used for CC09, with an initial surface crack length $c = 0.76\,\text{mm}$ and an aspect ratio of $a/c = 1$.

To assess the influence of load application on the results and to ensure a consistent comparison between the two software packages, a preliminary investigation was conducted in which the applied load position in ANSYS was varied. For the stress ratio $R = 0$, the load was initially applied at the top of the hole in ANSYS using two different approaches: one in which the load was distributed along a straight line defined by nodes at the top of the hole, and another in which the load was applied over a larger surface area represented by multiple elements at the top of the hole.

The difference between the two load application approaches used in the ANSYS simulations for $R = 0$ is illustrated in Figure 3.4.

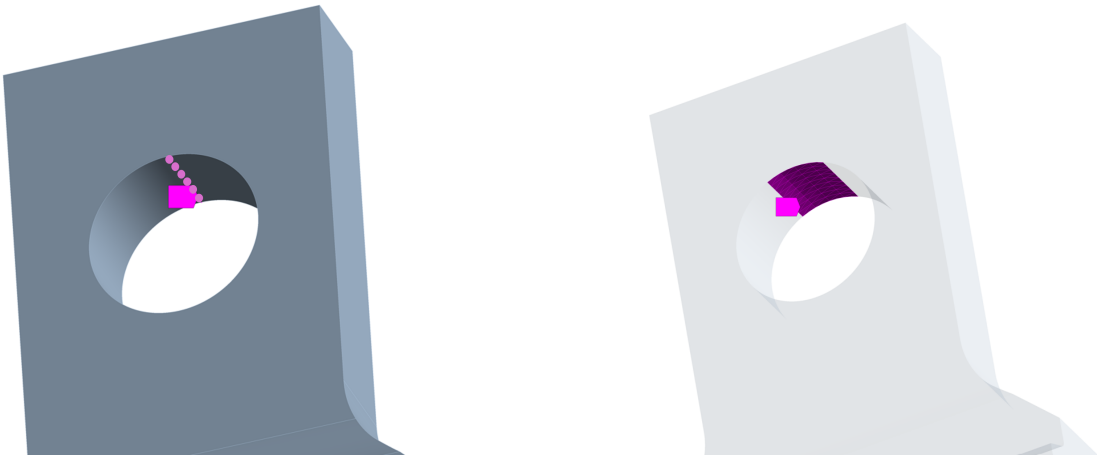

(a) **(b)**

Figure 3.4: Difference in the applied load definition in the ANSYS simulation of the lug for $R = 0$. **(a)**: Line load applied along nodes. **(b)**: Area load applied over surface elements.

The results, presented in Section 4.5, indicate that no significant differences were observed between the two load application approaches in ANSYS. Consequently, the nodal load application was adopted for the remaining simulations due to its simpler implementation. Furthermore, simulations with a stress ratio of $R = -1$ were also carried out in ANSYS as part of the investigation. In this case, sets of nodes were defined both at the top and bottom of the hole in the lug, and the location of the applied load was alternated between these locations for each half-cycle, illustrated in Figure 3.5.

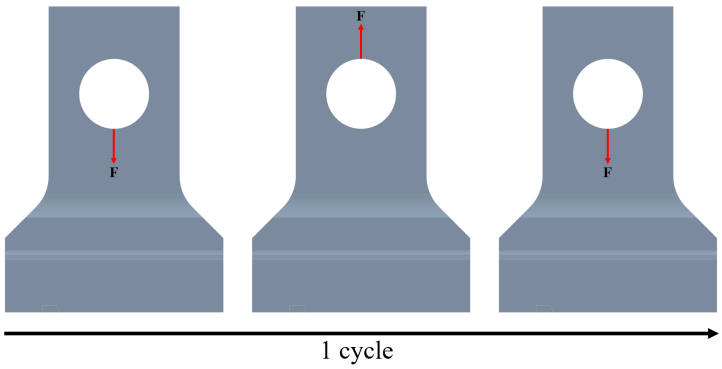

Figure 3.5: Load definition for the lug in ANSYS to represent a load case of $R = -1$.

For the reference cases on which NASGRO is based, the SIF is observed to increase when approaching the free surface and to decrease sharply at the surface itself. This surface boundary effect is expected but not yet fully understood; see Section 2.1.1.

For fatigue crack growth analyses of semi-elliptical surface cracks and quarter-elliptical corner cracks, NASGRO assigns the near-surface ΔK value to the surface

crack tip. To account for the surface boundary effects, this surface value is multiplied by the correction factor β when calculating the crack growth rate. The factor β is defined in NASGRO [4] as

$$\beta = \begin{cases} 0.9 + 0.2R^2 - 0.1R^4 & \text{if } R > 0 \\ 0.9 & \text{if } R \leq 0 \end{cases} \tag{3.2}$$

Simulations for $R = 0$ in NASGRO were performed both with and without the application of the β-factor.

For all simulations, the pin load magnitude was set to 40 kN. In NASGRO, the loading is defined as the nominal stress given by $S_3 = P/(Dt)$, where P is the applied force on the loading pin, yielding $S_3 \approx 277.78$ MPa. In both software packages, the loading was specified as purely tensile, and the direction of the force P was upwards with respect to Figures 3.3(a) and 3.3(b).

For the case of $R = -1$, NASGRO offers an option referred to as compression clipping. When this option is enabled, negative SIF values are set to zero in the crack growth calculations, resulting in behaviour equivalent to a stress ratio of $R = 0$. According to the NASGRO documentation, this approach provides a more physically realistic representation of the loading condition, as the negative load on the lug bore is expected to result in negligible stress on the crack plane. An user can opt for the option *full range* instead of compression clipping in NASGRO. However, in this case, NASGRO uses a stress intensity factor range that is double of what is obtained under the positive load, which is not physically realistic (see Figure 3.5). The effect of compression clipping was also investigated and included in the results for the lug geometry.

3.2 Simulation process in NASGRO

NASGRO is based on a large collection of reference FE solutions and employs calibrated geometry correction factors for each specific crack configuration. These geometry correction factors are combined with the applied loads to evaluate the SIFs, as described in Equation 2.4. For fatigue crack growth calculations, NASGRO utilises the NASGRO equation, see Equation 2.14, to compute the crack growth rate based on the calculated SIFs.

In this thesis, the programs NASSIF, used for efficient stress intensity factor calculations, and NASFLA, used for fatigue crack growth (FCG) analyses, were employed. The general workflow of a NASGRO analysis is illustrated in Figure 3.6.

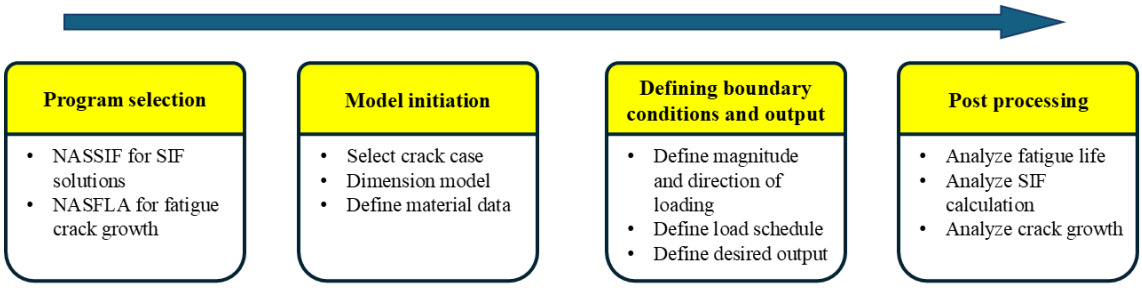

Figure 3.6: Flow chart illustrating the general NASGRO procedure.

After selecting the appropriate program for the desired fracture analysis, a crack configuration was chosen from the NASGRO library. The crack size, crack location, and specimen dimensions were then defined, subject to the standardised geometrical constraints and validity limits imposed by NASGRO.

Subsequently, the material properties were specified either by selecting a material from the built-in NASGRO material database or by defining the required material parameters manually. Once the geometry and material definitions were complete, the loading type and loading history were prescribed. Finally, the desired output options were selected, after which the analysis was executed and the results were obtained for further evaluation. This section describes the NASGRO implementation adopted in the present thesis work.

3.2.1 SIF solution in NASSIF

NASSIF calculations were performed for the cases specified in Section 3.1 in order to compute the SIFs for the initial crack sizes. NASGRO provides SIF solutions according to the formulations described in Section 2.2.1. For the cases investigated in this thesis, NASGRO calculated SIFs at two computational points along the crack front, which is assumed to correspond to the locations of maximum SIF values.

This assumption was validated by comparison with ANSYS solutions, for which SIFs were evaluated at multiple locations along the crack front. The orientation and location of the computational points used by NASGRO for the crack configurations investigated in this thesis are illustrated in Figure 3.7.

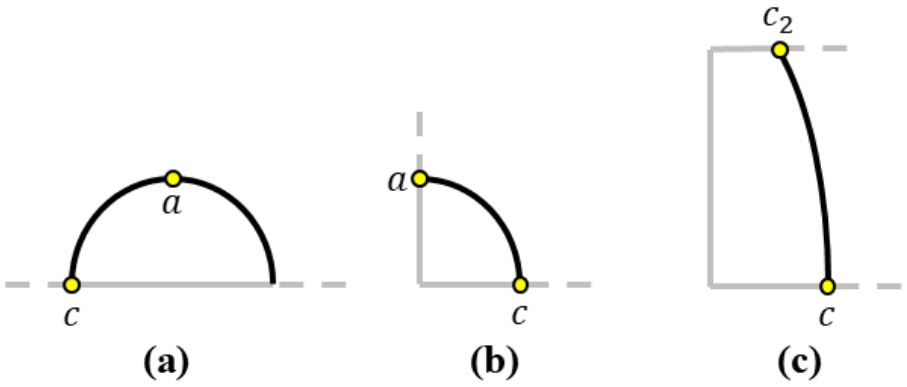

Figure 3.7: Orientation of calculation points in NASGRO for **(a):** Semi-elliptical surface crack SC30, **(b):** Quarter-elliptical corner crack CC09 and CC19, **(c):** Part-elliptical through crack TC45.

The SIFs at these computational points were evaluated for all cases and compared with the corresponding ANSYS results. In addition, the calculated SIFs were used as initial values for the FCG calculations during post-processing in order to examine the evolution of SIFs over the entire loading schedule, since the NASFLA module, in v.11.1, does not output the initial SIF values.

3.2.2 Fatigue crack growth simulation in NASFLA

NASFLA was used to calculate FCG using the SIF solving approach presented in Sections 2.2.1 and 3.2.1 at each increment of the analysis. At each step, NASFLA evaluated the crack growth increment based on the calculated SIFs and continued the simulation until a predefined stopping criterion was reached. For most cases, the analysis was terminated when the SIF exceeded the material fracture toughness, whereas for some cases the simulation stopped when the crack size exceeded the validity limits of the selected crack configuration.

3.2.2.1 Model set up

The models were set up according to the geometries presented in Section 3.1. The material used in all NASFLA simulations was Inconel 718 at room temperature (ID Q3LA12AB1), selected from the standard NASGRO material library. The modifications made to the material properties were that the fracture toughness was defined using the Mode I fracture toughness, denoted K_{1c} in NASGRO.

The loading schedules were defined according to Section 3.1.1.1. Although NASFLA allows simulations to be run for a predefined number of cycles, fatigue life solution was desired, and thus the simulations were ran until a stopping criterion was fulfilled. One stopping criterion available in NASGRO is net-section stress exceeding a critical value, where, net-section stress is generally expressed as [4]

$$S_n = \frac{P}{A_n} + \frac{Mc}{I_n} \tag{3.3}$$

where A_n and I_n are the net-section area and second moment of area, respectively, P is the resultant axial force, M is the resultant bending moment, and c denotes the distance to the outer fibres. However, in order to focus on the onset of unstable crack growth, this stopping criterion was bypassed in the current work.

Finally, the desired output options were specified. For convenience, the results were printed at a crack growth interval of 0.1 mm and to reduce computational time, especially for TC45 which were quite costly, the built-in *express mode*, was used. When this mode was enabled, the geometry correction factors in the SIF calculations were updated only at user-defined crack growth increments rather than at every simulation step. This resulted in a substantial reduction in computational time, while previous studies have shown that the associated loss of accuracy does not exceed approximately 1% [4]. Once the full model was defined, the simulations were executed and the results were obtained.

3.2.2.2 Transition modelling

The NASGRO implementation of crack transition from a corner crack to a through crack was described in Section 2.3.3.1. In NASGRO, two crack cases representing the quarter-elliptical corner crack geometry investigated in this thesis are available: CC01 and CC09. The primary difference between these cases is that CC09 supports arbitrary bivariant loading, whereas CC01 is restricted to predefined loading conditions, such as tension and bending. In addition, the post-transition crack geometry associated with CC01 is the part-elliptical through crack case TC47, whereas CC09 transitions to TC45. The TC45 and TC47 geometries are identical in shape; however, TC47 does not permit through-width (in-plane) bending.

Regarding the built-in transition criteria in NASGRO, the full thickness-penetration criterion is used for the CC01 $\rightarrow$ TC47 transition, while the 95% thickness criterion is used for the CC09 $\rightarrow$ TC45 transition. A comparison between the two transition algorithms was performed using a tensile cyclic loading of $S_{\max} = 300\,\text{MPa}$ with a stress ratio of $R = 0$, based on the geometry defined in Section 3.1.The purpose of this comparison was to distinguish any differences in predicted fatigue life arising from the different transition models. The resulting final crack shapes are illustrated in Figure 3.8. For reference, the same configuration was also modelled in ANSYS as described in Section 3.3, and the corresponding result is included in the figure.

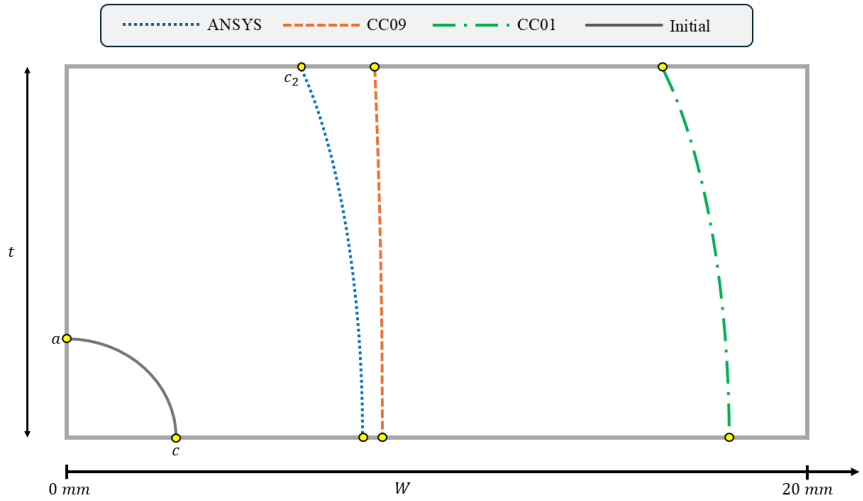

Figure 3.8: Illustration of end-of-life crack shape after transition of a quarter-elliptical corner crack.

As shown, significant differences in crack size at termination were observed between the simulations. Both the ANSYS simulation and the NASGRO CC09 analysis were terminated when the SIF exceeded the fracture toughness, occurring at 256 500 and 271 082 cycles, respectively. In contrast, the NASGRO CC01 simulation kept the crack growing and terminated because the crack length exceeded the admissible range, $\frac{c}{W} \leq 0.9$, at 321 305 cycles.

To further investigate the origin of these differences, the evolution of SIFs with crack extension at the computational points defined in Figure 3.7 were also compared. These results are shown in Figure 3.9.

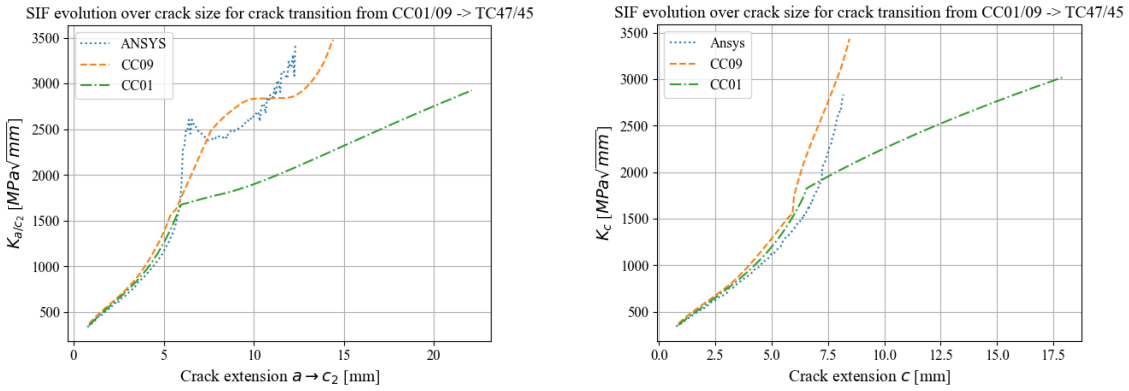

(a) **(b)**

Figure 3.9: SIF over crack extension at the **(a)**: a-node for a corner crack transitioning to c_2 for a through crack. **(b)**: c-node for a corner crack transitioning to a through crack.

The pre-transition SIF trends were similar for all approaches, whereas significant differences were observed after transition. The CC01/TC47 configuration yielded

systematically lower SIF values, while the CC09 and ANSYS results showed close agreement. This explains the larger crack size obtained for the CC01 configuration.

To determine whether this discrepancy originated from the transition model or from the post-transition SIF formulation, additional simulations were performed using TC45 and TC47 as standalone through-crack models, initialised with the crack dimensions immediately after transition. The resulting SIF evolution is shown in Figures 3.10(a) and 3.10(b).

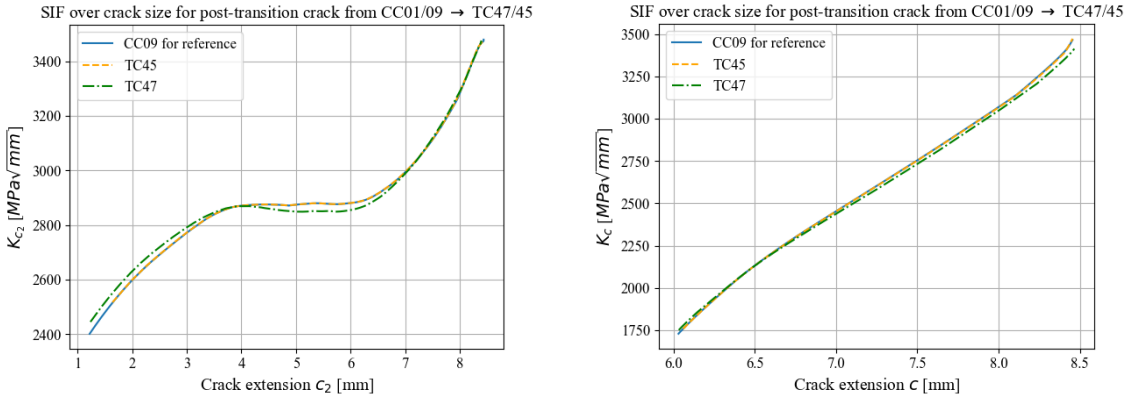

(a) **(b)**

Figure 3.10: SIF over crack extension at the **(a)**: c_2-node post-transition from a corner crack to a through crack. **(b)**: c-node post-transition from a corner crack to a through crack.

The results showed that standalone through-crack simulations in NASGRO produced nearly identical SIF evolutions for the TC45 and TC47 configurations. Consequently, it was concluded that the discrepancies observed in Figures 3.9(a) and 3.9(b) originated from differences in the transition and post-transition SIF formulations applied in the CC01 and CC09 models, rather than from the through-crack formulations themselves. Since the CC09 results showed close agreement with ANSYS and the standalone through-crack simulations, the CC09 configuration was selected for all NASGRO analyses of quarter-elliptical corner cracks in this thesis.

3.3 Simulation process in ANSYS

All simulations were performed using ANSYS Workbench, with the setup and solution procedures carried out in ANSYS Mechanical. For each simulation, the preprocessing stage consisted of defining the engineering data, geometry, and model setup. The overall simulation workflow, together with the most relevant settings, is described in this section. A schematic representation of the general simulation procedure in ANSYS is provided in Figure 3.11.

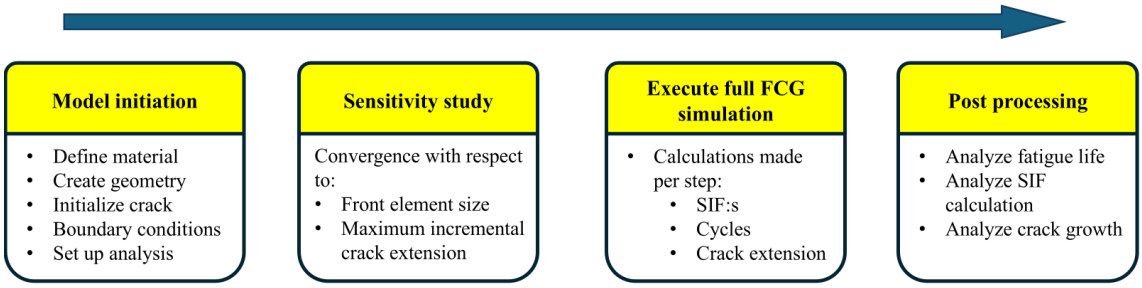

Figure 3.11: Flow chart of the general ANSYS procedure.

3.3.1 Sensitivity study

A sensitivity study was conducted to ensure that the numerical results obtained were sufficiently accurate and converged. The selection of parameters in the sensitivity study was guided by considerations of mesh feasibility, reasonable computational time, and convergence of the results. Two parameters of particular importance when modelling crack propagation in ANSYS were examined. The first parameter was the crack front element size, while the second was the maximum incremental crack extension, which controls the allowable crack growth per simulation step.

3.3.1.1 Front element size

The crack front element size was varied for all crack types in order to assess convergence. Convergence was evaluated based on the SIF distributions along the crack front. In ANSYS, the SIFs are calculated using contour integrals, where each contour represents a specified radial distance from the crack front. Within the SMART crack growth tool, both the number of contours and the maximum contour radius can be defined. For all crack cases, the number of contours was set to six, and the maximum contour radius was chosen to be at least six times the crack front element size, to ensure at least one element in each contour. To assess the adequacy of a given front element size, convergence was considered to be achieved when at least two of the six contour plots overlapped, indicating mesh-independent SIF results.

The sensitivity study for the crack front element size was conducted consistently for all crack cases. Convergence was assessed under static tensile loading. As no crack growth occurs under static loading, the results were independent of the maximum incremental crack extension parameter. The crack front element size was varied across the following values: 0.2 mm, 0.1 mm, 0.05 mm, 0.025 mm, and 0.0125 mm. The values lie between 0.522% to 8.377% of the initial crack front length for SC30. For CC09 and lug they lie between 1.047% to 16.75%, and for TC45 between 0.206% to 3.293%. The values were chosen to ensure a balance between sufficient resolution and a reasonable computational time for the simulations. The maximum contour radius was adjusted accordingly for each element size. The resulting SIF distributions used to assess convergence for all crack cases are presented in Figure 3.12.

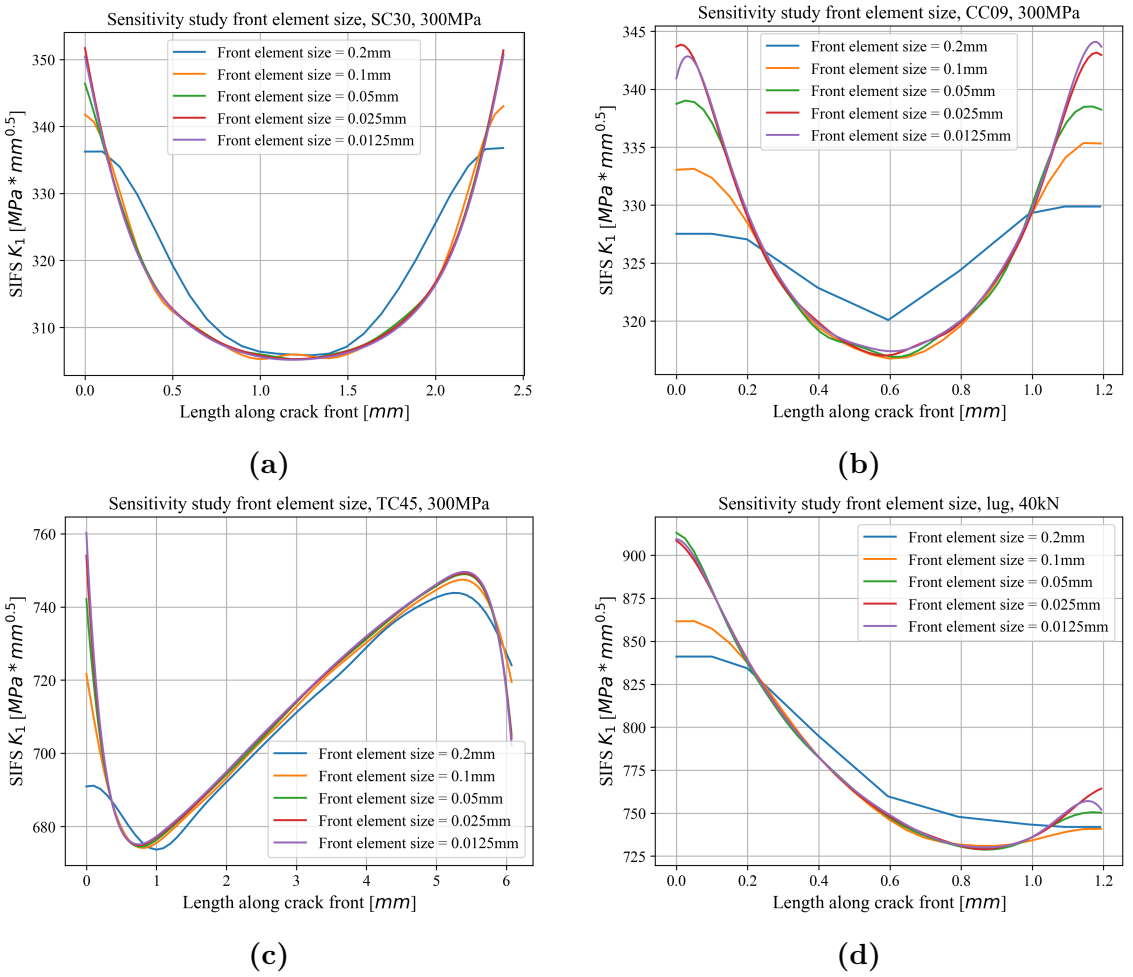

Figure 3.12: SIF evaluation along the crack front in ANSYS for different front element sizes. Evaluated for all crack cases. **(a):** SC30. **(b):** CC09. **(c):** TC45. **(d):** Lug.

The convergence behaviour was found to be similar for all four crack cases. Slower convergence were observed in the SIF values at the free surface for the majority of the crack configurations. This behaviour may be attributed to the breakdown of the classical $1/\sqrt{r}$ singularity assumption, which is no longer valid in this region of the crack front [19]. The most consistent convergence was observed for a crack front element size of 0.025 mm, which produced results comparable to those obtained with the finest mesh size of 0.0125 mm. However, when accounting for computational cost, and considering that convergence in the interior region of the crack front was of greater significance, particularly given the convergence difficulties at the boundaries, a larger element size was determined to be more appropriate. Consequently, a crack front element size of 0.05 mm was selected for the subsequent fatigue crack growth simulations, as it provided sufficient accuracy while offering improved computational efficiency. This corresponds to about 6.5 % of the initial crack size 0.76 mm used in most simulations.

3.3.1.2 Maximum incremental crack extension

The maximum incremental crack extension was the second parameter investigated in the sensitivity study. Fatigue crack growth simulations were performed under tensile loading with $R = 0$ to evaluate the effect of this parameter on crack growth behaviour. The comparison for these simulations was performed based on crack extension as a function of the number of load cycles, since life-time prediction constitutes the primary quantity of interest. The following values were examined for the maximum incremental crack extension: 0.15 mm, 0.1 mm, and 0.05 mm. As crack growth occurs in these simulations, the maximum incremental crack extension was defined as a control parameter within the SMART crack growth tool. The resulting crack growth curves for SC30, CC09, TC45 and CC19 are presented in Figures 3.13 - 3.16.

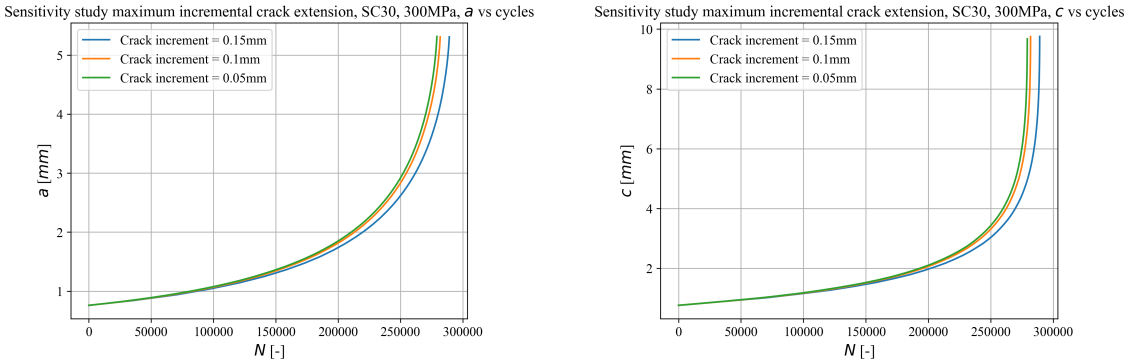

(a) **(b)**

Figure 3.13: Crack extension vs number of cycles in ANSYS for different maximum incremental crack extension, for SC30. **(a)**: a vs N. **(b)**: c vs N.

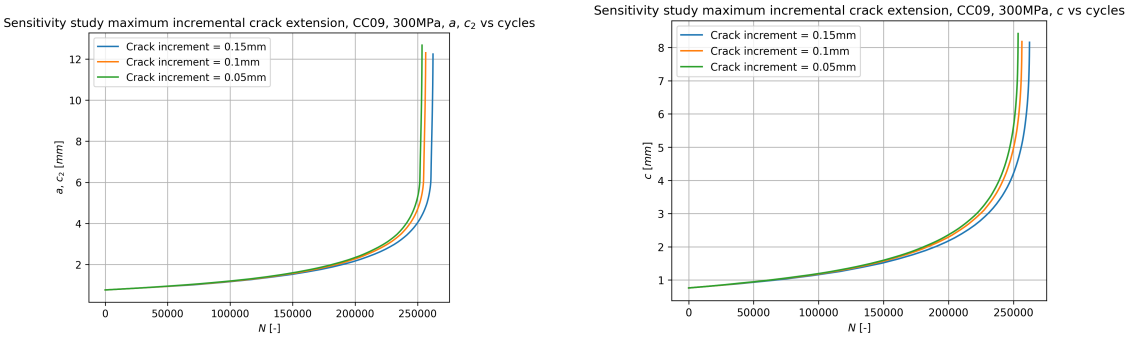

(a) **(b)**

Figure 3.14: Crack extension vs number of cycles in ANSYS for different maximum incremental crack extension, for CC09. **(a)**: $a \rightarrow c_2$ vs N. **(b)**: c vs N.

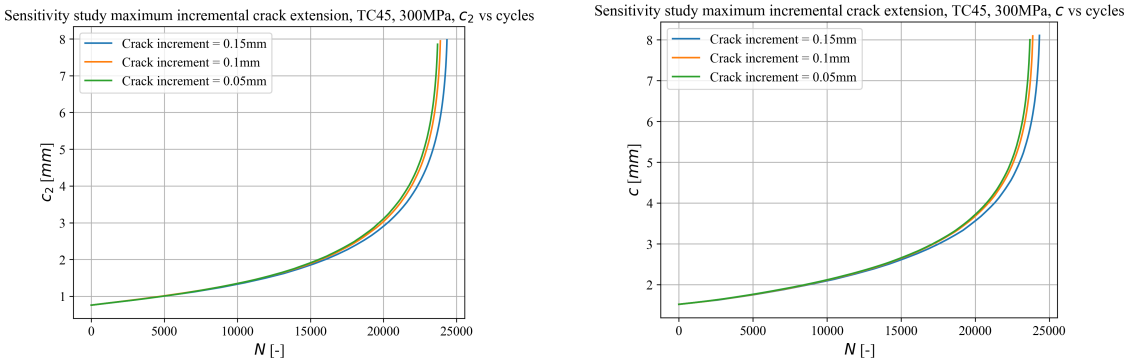

(a) **(b)**

Figure 3.15: Crack extension vs number of cycles in ANSYS for different maximum incremental crack extension, for TC45. **(a)**: c_2 vs N. **(b)**: c vs N.

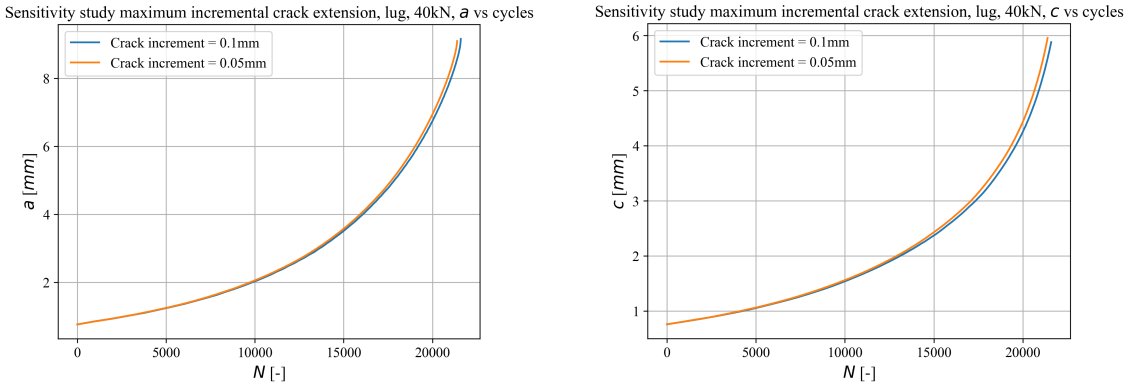

(a) **(b)**

Figure 3.16: Crack extension vs number of cycles in ANSYS for different maximum incremental crack extension, for CC19. **(a)**: a vs N. **(b)**: c vs N.

The results indicate a small dependence on the chosen crack extension increment value, with finer extensions generally resulting in a lower predicted number of life cycles. For a maximum incremental crack extension of 0.15 mm, the increment value exceeded twice the selected crack front element size, and moderate mesh coarsening was therefore applied. In the case of the lug geometry, moderate mesh coarsening led to remeshing errors, which is consistent with the recommendation that conservative coarsening is preferable to maintain numerical stability. This is the reason why only increment values of 0.1 mm and 0.05 mm are presented for the lug case. A small difference in the final crack size was observed for the finest step size. Despite this difference, a maximum incremental crack extension of 0.1 mm was considered sufficient to achieve convergence in both predicted number of cycles and the final crack dimensions. The discrepancy relative to the 0.05 mm case was deemed acceptable, particularly given the substantially increased computational time associated with the smallest increment value.

3.3.2 Interpretation of R-ratio in ANSYS

As described in Section 2.3, the stress ratio R influences the fatigue crack growth rate. In the SMART module in ANSYS, a stress ratio R was defined; however, during the simulations it was observed that the specified R was only used within the crack growth law for evaluating $\frac{da}{dN}$ and did not correspond to an explicitly applied reversed loading condition for $R < 0$. This limitation is particularly relevant for through-thickness bending of through cracks, where different parts of the crack front may open and close during different stages of a fully reversed loading cycle.

To simulate a fully reversed loading cycle ($R = -1$), non-proportional cyclic loading commands, CLOAD and NPLOAD, were implemented in ANSYS using an APDL-based approach. For a detailed explanation of the relevant commands used, see Appendix B. This required an extension of the SIF range calculations used in the crack growth law. A limitation encountered in ANSYS SMART was that negative SIF values were not permitted, which would otherwise occur during the compressive part of the loading cycle. In such cases, the effective SIF range was internally truncated according to

$$\Delta K = \begin{cases} K_{max} - K_{min} & \text{if } K_{min} > 0 \\ K_{max} & \text{if } K_{min} \leq 0 \end{cases} \tag{3.4}$$

As a consequence, even when a fully reversed loading cycle was defined using CLOAD, the crack growth calculation in SMART only accounted for the tensile portion of the loading cycle. To better represent the $R = -1$ condition within the crack growth law, SIFs were calculated using the bulit-in method based on mode-separation (CGROW, NPLOAD, METH, DKMOD) [6]. However, the SMART algorithm still truncated negative SIF values according to Equation 3.4. This approach nevertheless allowed a user-defined stress ratio to be applied within the crack growth law in the SMART module.

Despite the truncation of negative SIF values, the crack growth calculations showed good agreement with NASGRO when using the DKMOD method, where the stress ratio R is explicitly defined in the SMART interface. This behaviour can be understood by considering that the effective SIF range in the NASGRO equation can be reformulated as

$$\Delta K_{\text{eff}} = \left[\frac{1-f}{1-R}\Delta K\right] = \left[\frac{1-f}{1-R}K_{\max}(1-R)\right] = [(1-f)K_{\max}] \tag{3.5}$$

Thus, the dependence on ΔK could be effectively replaced by $K_{\max}$ when crack closure effects are considered, making the truncation of $K_{\min}$ less influential under these conditions.

A comparison between this APDL-based implementation and a standard reversed loading setup defined directly within the SMART module was performed. In cases where the default SMART implementation did not adequately represent the intended

loading conditions, the CLOAD/NPLOAD approach was used for the comparison between ANSYS and NASGRO.

3.3.3 Surface effects study

When calculating SIFs, it has previously been noted that a different singularity exists at locations where the crack front intersects a free surface boundary. In Section 2.1.1, the theoretical background related to surface effects is discussed in more detail, including the observation that it is not explicitly stated how ANSYS accounts for these effects in its SIF calculations. The objective of the present section is therefore to investigate how surface effects may be treated in ANSYS. Based on the discussion in Section 2.1.1, both Poisson's ratio and the crack front intersection angle with the free surface are expected to influence the SIF behaviour near the boundary. To examine potential trends, a series of static loading simulations were performed in which Poisson's ratio was varied between $\nu = 0.29$ and $\nu = 0$ for through cracks with different intersection angles at the free surface. While this study did not allow for the derivation of an explicit formulation or definitive method describing how ANSYS incorporates surface effects into its SIF calculations, it enabled qualitative conclusions to be drawn regarding dependencies and trends consistent with the theoretical considerations presented in Section 2.1.1.

As an initial step, the through crack configurations investigated in this study were defined. The corresponding geometries are shown in Figure 3.17, together with the notation used for the two crack cases considered. The primary difference between these crack geometries lies in the intersection angle between the crack front and the free surface. For the straight crack front case, the crack front intersects the boundary orthogonally, whereas the angled crack front case exhibits a non-orthogonal intersection. In the angled crack front configuration, the initial value of c_2 was kept identical to that of the straight crack front case, while the crack length c was adjusted to achieve an initial aspect ratio of $c_2/c = 0.5$. The normal stress was evaluated at 50% of c_2 corresponding to 0.32 mm ahead of the crack front. The resulting distributions of SIFs and normal stress along the crack front are presented in Figures 3.18 - 3.19. These figures compare results obtained for different values of Poisson's ratio under tensile loading of 400 MPa.

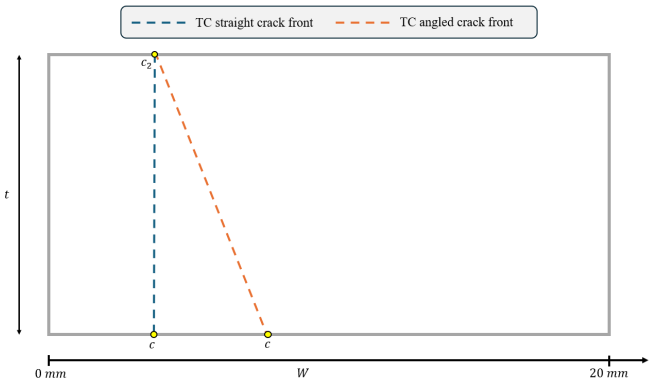

Figure 3.17: Illustration of straight and angled crack fronts of a through crack.

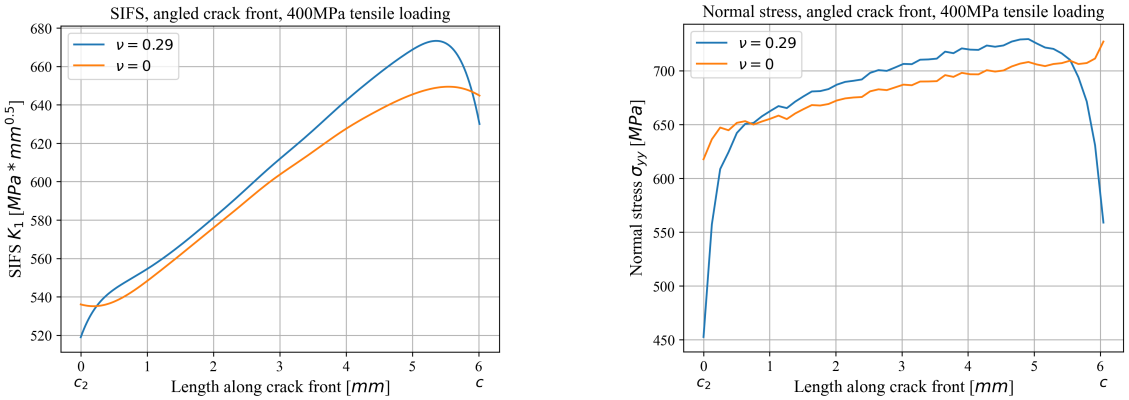

(a) **(b)**

Figure 3.18: Effect of Poisson's ratio on **(a)**: SIF and **(b)**: normal stress, for an angled crack front.

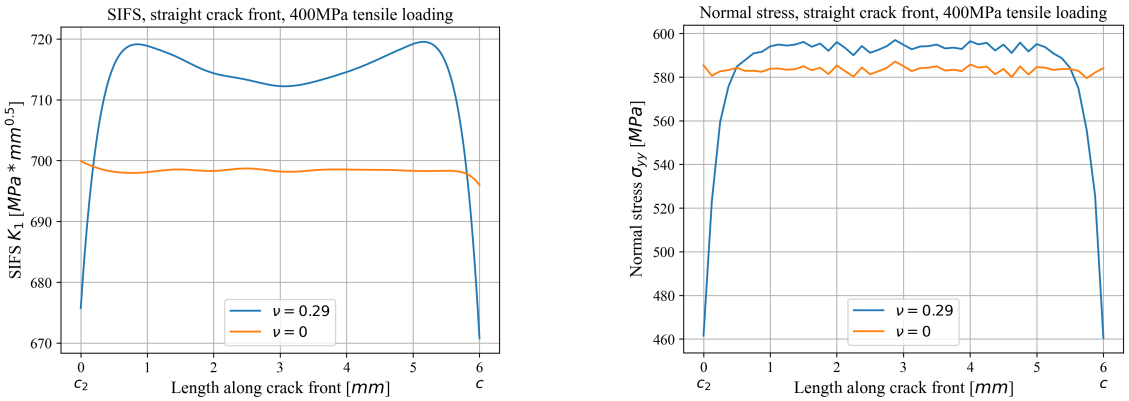

(a) **(b)**

Figure 3.19: Effect of Poisson's ratio on **(a)**: SIF and **(b)**: normal stress, for a straight crack front.

The plots indicate that the reduction in normal stress near the free surface corresponds closely to the observed decrease in the calculated SIFs. The dependence on Poisson's ratio shows trends that are in qualitative agreement with the theoretical boundary layer behaviour discussed in Section 2.1.1. However, variations in the crack front intersection angle do not exhibit the expected influence based on the same theoretical framework. This suggests that ANSYS employs a separate treatment for the evaluation of SIFs at the crack front boundary located at the free surface. While such a distinction in the intersection angle appears to be present, the observed behaviour does not fully conform to the analytical formulation introduced in the theory chapter. It is therefore not possible to determine the exact nature of the underlying calculation procedure in ANSYS, but the results indicate that it differs from the theoretical description.

3.4 Comparison process

The post-processing phase primarily consisted of a systematic comparison between the two software packages, focusing on fatigue life predictions, evolution of SIF values, and crack front aspect ratios obtained from the fatigue simulations. For each crack configuration and loading condition, corresponding results from NASGRO and ANSYS were compared directly. The principal output parameters considered in the analysis were crack dimensions, number of load cycles, and SIF values. The results were organized and evaluated according to the following categories:

- Crack length vs number of cycles (a, c, c_2 vs N)
- SIFs vs crack length (K_a vs a, K_c vs c and K_{c_2} vs c_2)
- Aspect ratio vs crack extension at c-node (a/c vs c and c_2/c vs c)

In addition to the numerical comparison, qualitative aspects related to user-friendliness were also considered. This assessment is presented in the conclusions and is based on documentation, usability observations, and workflow experience recorded for each crack case and software throughout the study.

4

Results

In this chapter, the results obtained from all simulated crack propagation cases are presented. The results are presented in terms of the quantities identified in Section 3.4 illustrated through comparative plots. The studied crack configurations are in NASGRO denoted as SC30, CC09, TC45 and CC19. A detailed illustration of the geometries of these cases can be found in the NASGRO manual [4]. A general discussion and significance of these results are provided in Chapter 5.

4.1 Semi-elliptical surface crack (SC30)

This section presents the results obtained for the SC30 crack configuration. The corresponding results for tensile loading $S_0 = 300\,\text{MPa}$ and $R = 0$ are shown in Figure 4.1.

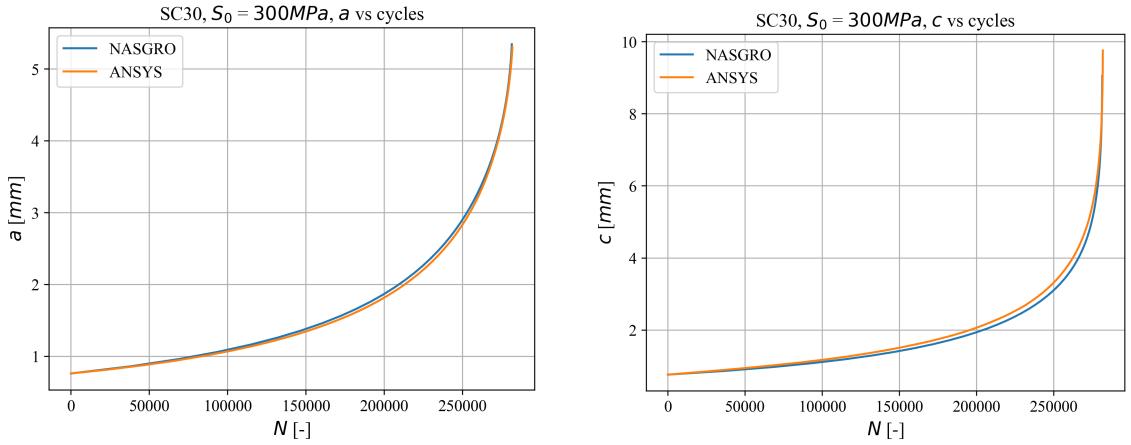

(a) **(b)**

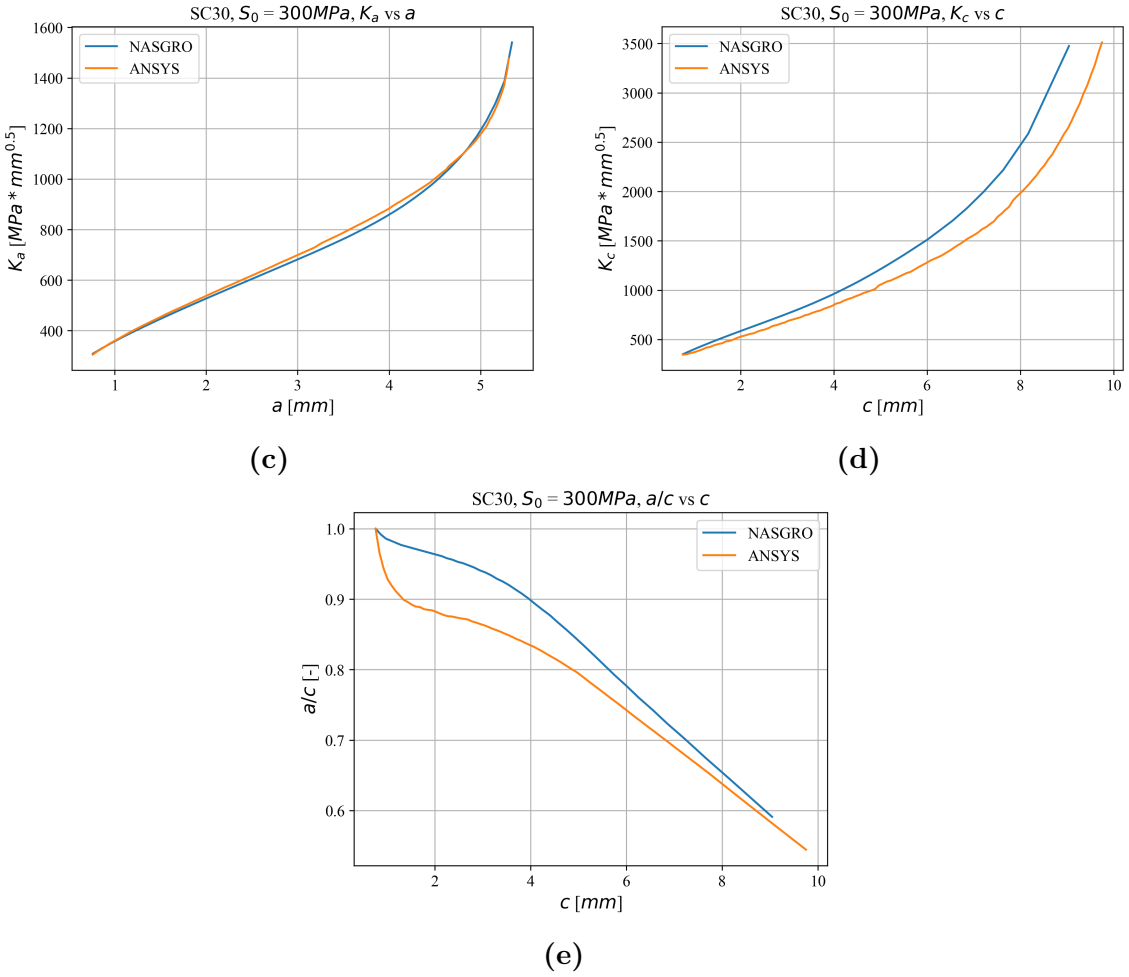

Figure 4.1: Comparison between NASGRO and ANSYS, for SC30 with $S_0 = 300\,\text{MPa}$, $R = 0$ loading. **(a)**: a vs N. **(b)**: c vs N. **(c)**: K_a vs a. **(d)**: K_c vs c. **(e)**: a/c vs c.

For the SC30 crack configuration subjected to S_0 loading, the results indicate very similar behaviour between NASGRO and ANSYS. The predicted SIFs, crack length evolution, and final number of load cycles show only minor differences, with the exception that ANSYS predicts slightly lower SIF values at a specific c-node crack length. However, for this crack case, NASGRO applies the surface constraint factor β to the SIFs when calculating the crack growth rate which results in the similar life predictions.

The results for bending loading $S_1 = 400\,\text{MPa}$ and $R = 0$ are shown in Figure 4.2.

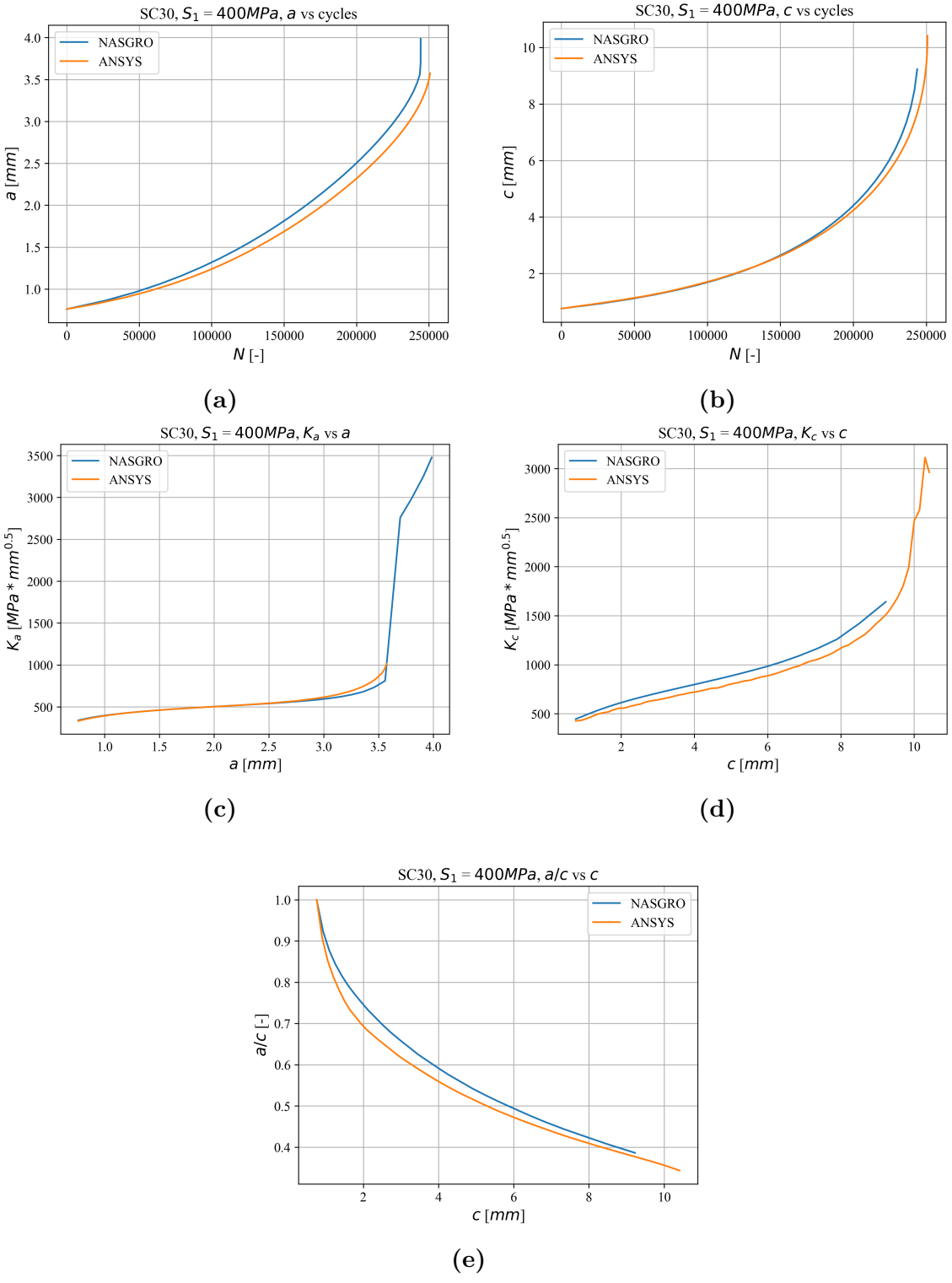

Figure 4.2: Comparison between NASGRO and ANSYS, for SC30 with S_1 = 400 MPa, $R = 0$ loading. **(a)**: a vs N. **(b)**: c vs N. **(c)**: K_a vs a. **(d)**: K_c vs c. **(e)**: a/c vs c.

For the SC30 with S_1 loading case, the results show good agreement between AN-

SYS and NASGRO in terms of SIFs, crack length evolution, and number of cycles to failure. A transition of the crack geometry is observed in this case, and it is in connection with this transition that the most pronounced differences between the two software packages can be identified. NASGRO predicts slightly more conservative number for cycles to failure. These discrepancies arise from the different approaches adopted by ANSYS and NASGRO in defining and handling crack transition.

The post-transition crack configuration of SC30 under these conditions is defined as a straight through crack in NASGRO. This implies that the crack front is described solely by the crack depth a, forcing the entire crack front to adopt a uniform value equal to a at the point of transition. Under S_1 bending, this leads to a rapid increase in the calculated SIFs, which reach the fracture toughness shortly after transition. This behaviour is a direct consequence of enforcing a straight through crack geometry. An option exists to select a curved through-crack as the post-transition crack configuration. However, in this case, this is only possible if the a-node penetrates the thickness rather than c reaching the width. For the thickness-penetration case, the crack will transition to TC29 [26]. For the simulated case, the c-node penetrates the width resulting in that only a straight crack front evolution is possible post-transition.

4.2 Quarter-elliptical corner crack (CC09)

For a corner crack, results for tensile loading with $S_0 = 300\,\text{MPa}$ and $R = 0$ are presented in Figure 4.3.

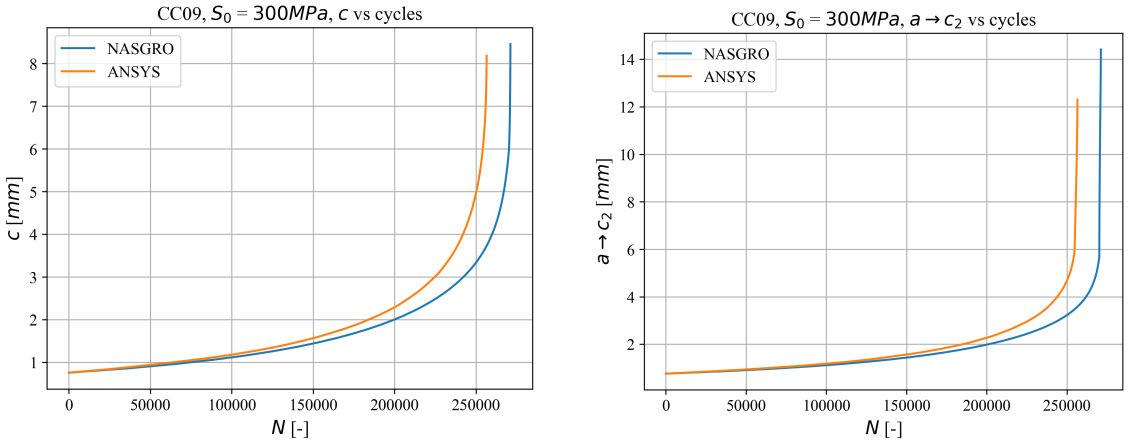

(a) **(b)**

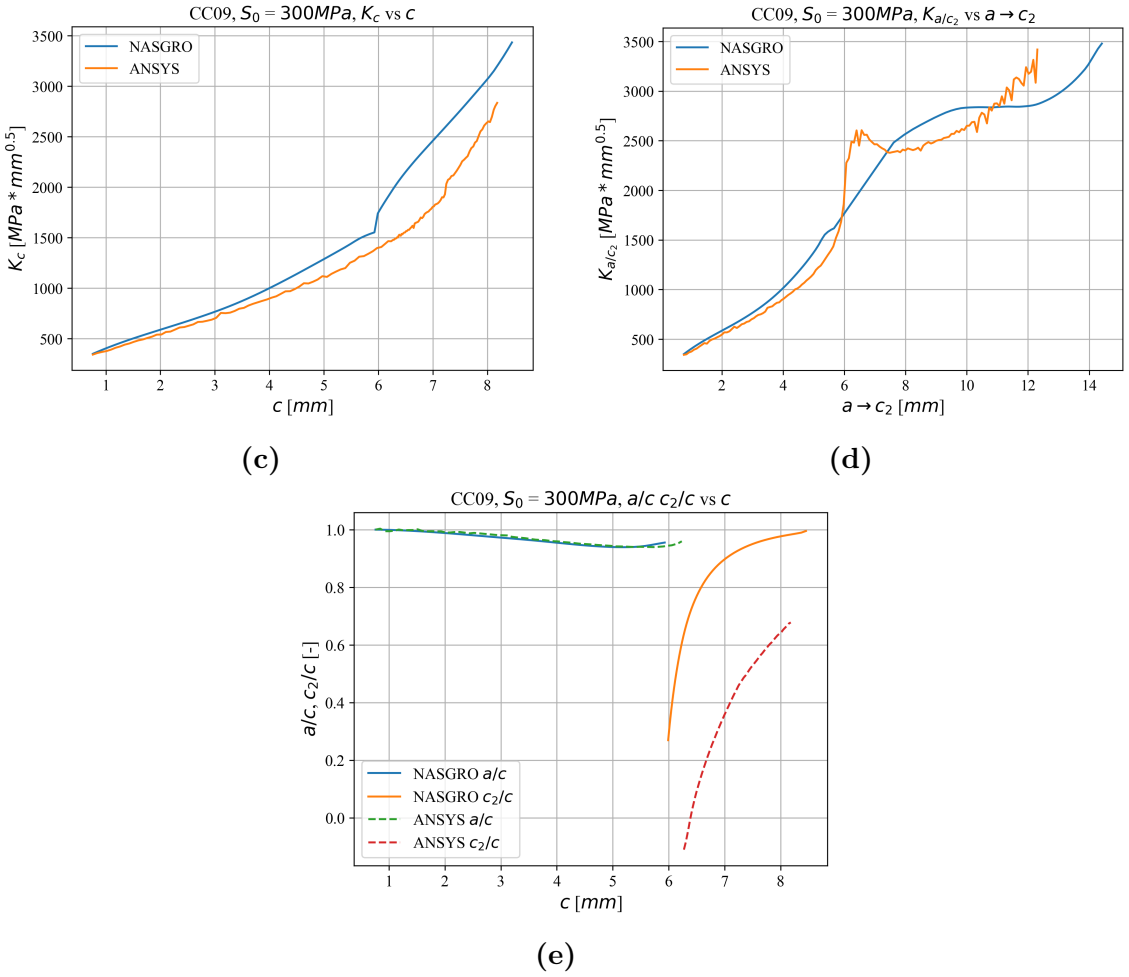

Figure 4.3: Comparison between NASGRO and ANSYS, for CC09 with $S_0 = 300\,\text{MPa}$, $R = 0$ loading. **(a)**: c vs N. **(b)**: $a \rightarrow c_2$ vs N. **(c)**: K_c vs c. **(d)**: $K_a \rightarrow K_{c_2}$ vs $a \rightarrow c_2$. **(e)**: $(a \rightarrow c_2)/c$ vs c.

The results show that the SIF evolution and fatigue life predictions obtained from ANSYS and NASGRO follow similar trends, with generally good agreement between the two software packages. However, ANSYS predicts slightly more conservative fatigue life. Differences are also observed in the crack shape evolution and the corresponding SIFs, which can be attributed to the different transition modelling approaches employed in the two tools. NASGRO employs an instantaneous transition into a curved through crack, TC45 geometry with $c_2 = 0.2c$, whereas ANSYS continuously evolves the crack shape during transition.

Results for through-thickness bending with a moment of $M_1 = 36\,000\,\text{Nmm}$ and $R = 0$ are presented below. This loading corresponds to a maximum nominal gross stress of $S_1 = 300\,\text{MPa}$ at the specimen edges. The results are shown in Figure 4.4.

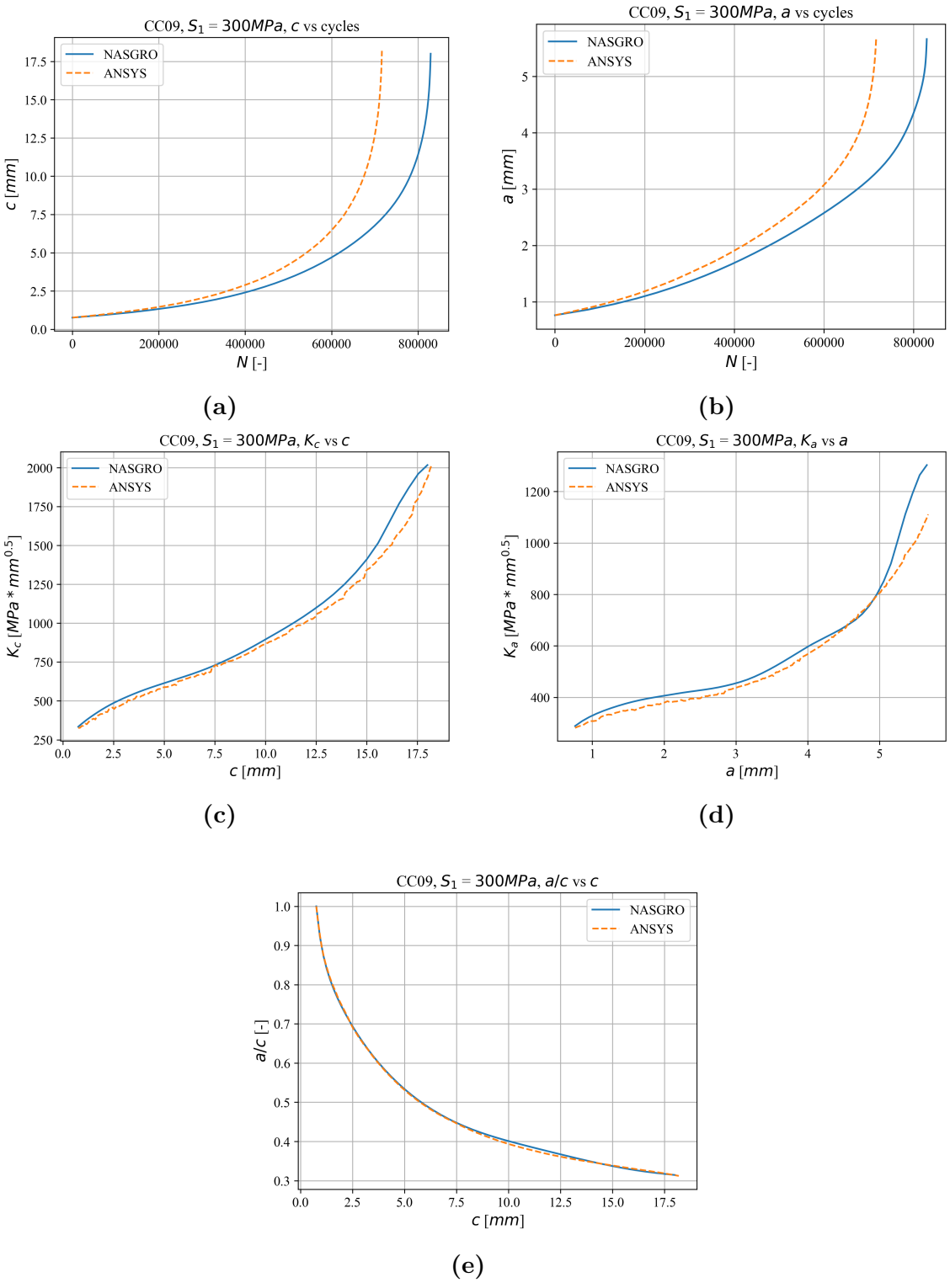

Figure 4.4: Comparison between NASGRO and ANSYS for CC09 under through-thickness bending corresponding to $S_1 = 300\,\text{MPa}$, $R = 0$. **(a)**: c vs N. **(b)**: $a \to c_2$ vs N. **(c)**: K_c vs c. **(d)**: $K_a \to K_{c_2}$ vs $a \to c_2$. **(e)**: $(a \to c_2)/c$ vs c.

For this case, ANSYS predicts a more conservative fatigue life. No crack transition

occurred, resulting in very similar aspect ratios throughout the simulation. The simulations were not terminated due to the fracture toughness being reached, but rather due to geometrical limitations of the crack configuration in NASGRO. An identical termination criterion was manually imposed in ANSYS to ensure consistent comparison between the results.

Results for in-plane bending with a moment of $M_2 = 120\,000\,\text{Nmm}$ and $R = 0$ are presented below. This loading also corresponds to a maximum nominal gross stress of $S_2 = 300\,\text{MPa}$ at the specimen edges. The results are shown in Figure 4.5.

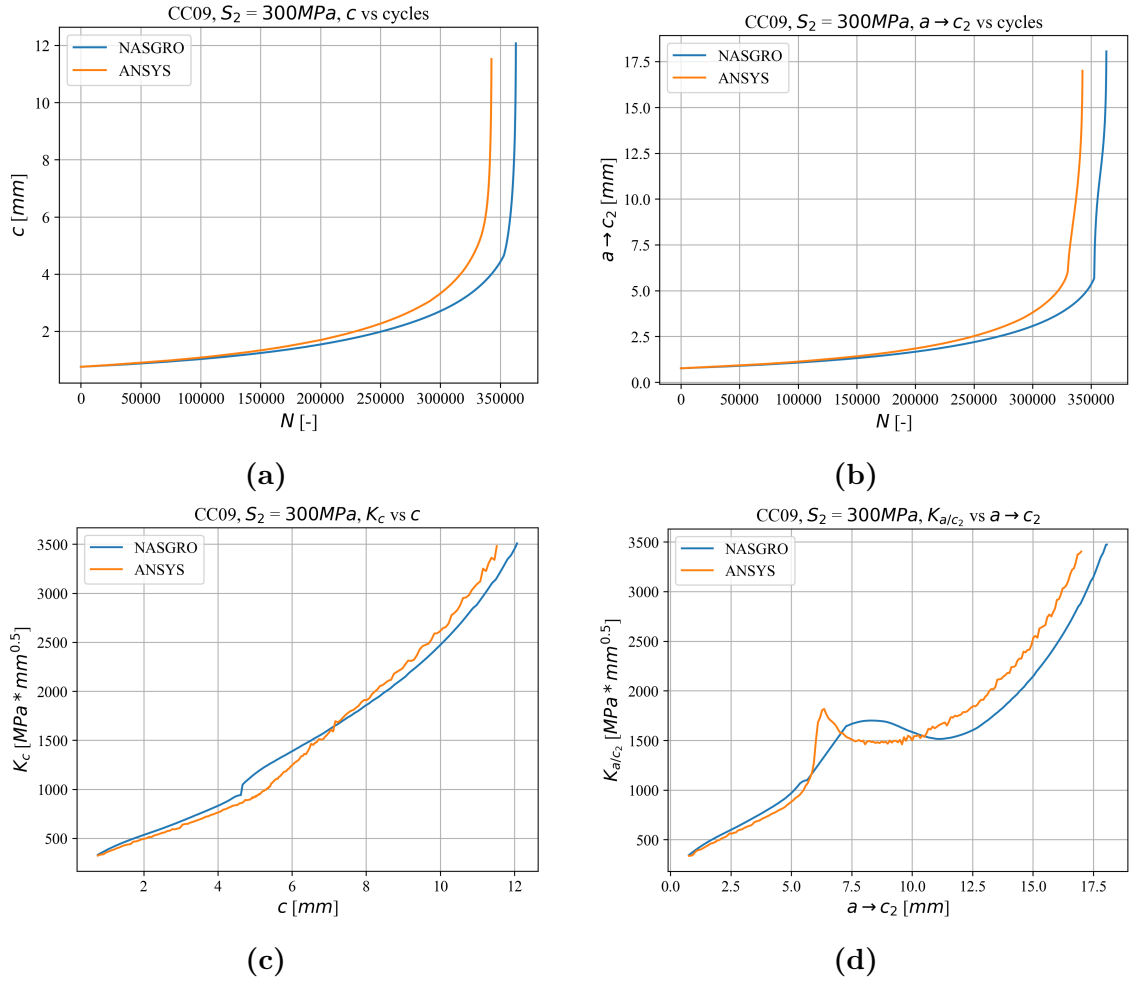

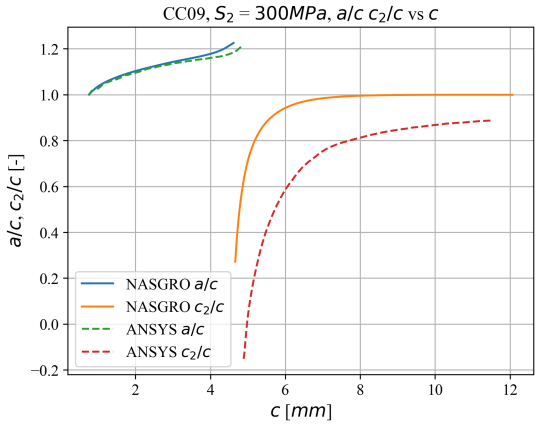

(e)

Figure 4.5: Comparison between NASGRO and ANSYS for CC09 under through-width bending corresponding to $S_2 = 300\,\text{MPa}$, $R = 0$.**(a)**: c vs N. **(b)**: $a \to c_2$ vs N. **(c)**: K_c vs c. **(d)**: $K_a \to K_{c_2}$ vs $a \to c_2$. **(e)**: $(a \to c_2)/c$ vs c.

Although the absolute results differ, the trends observed are similar to those obtained under tensile loading conditions. ANSYS consistently predicted slightly more conservative fatigue lives. Differences were also observed in the aspect ratio evolution which can be attributed to the different transition modelling approaches employed in the two tools.

4.3 Part-elliptical through crack (TC45)

This section presents the results obtained for the TC45 crack configuration. The corresponding results for tensile loading, $S_0 = 300\,\text{MPa}$, $R = 0$, are shown in Figure 4.6.

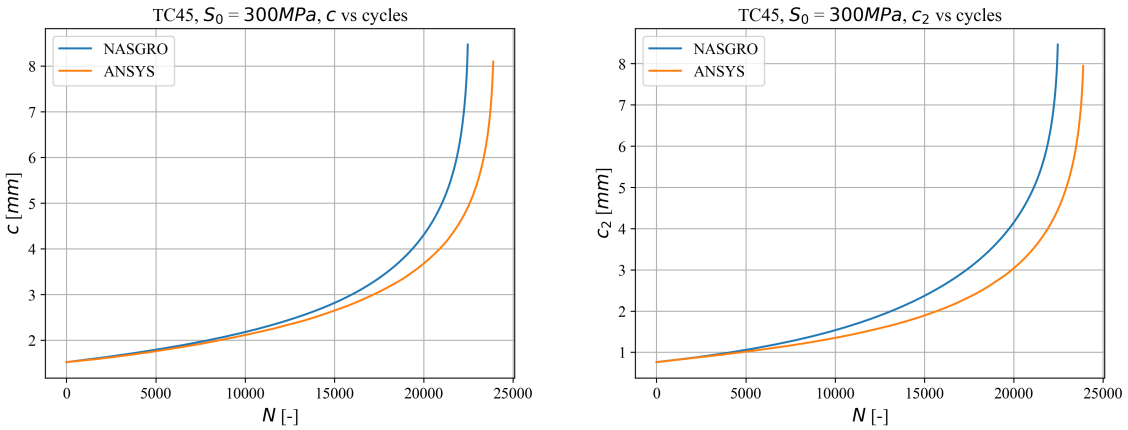

(a) **(b)**

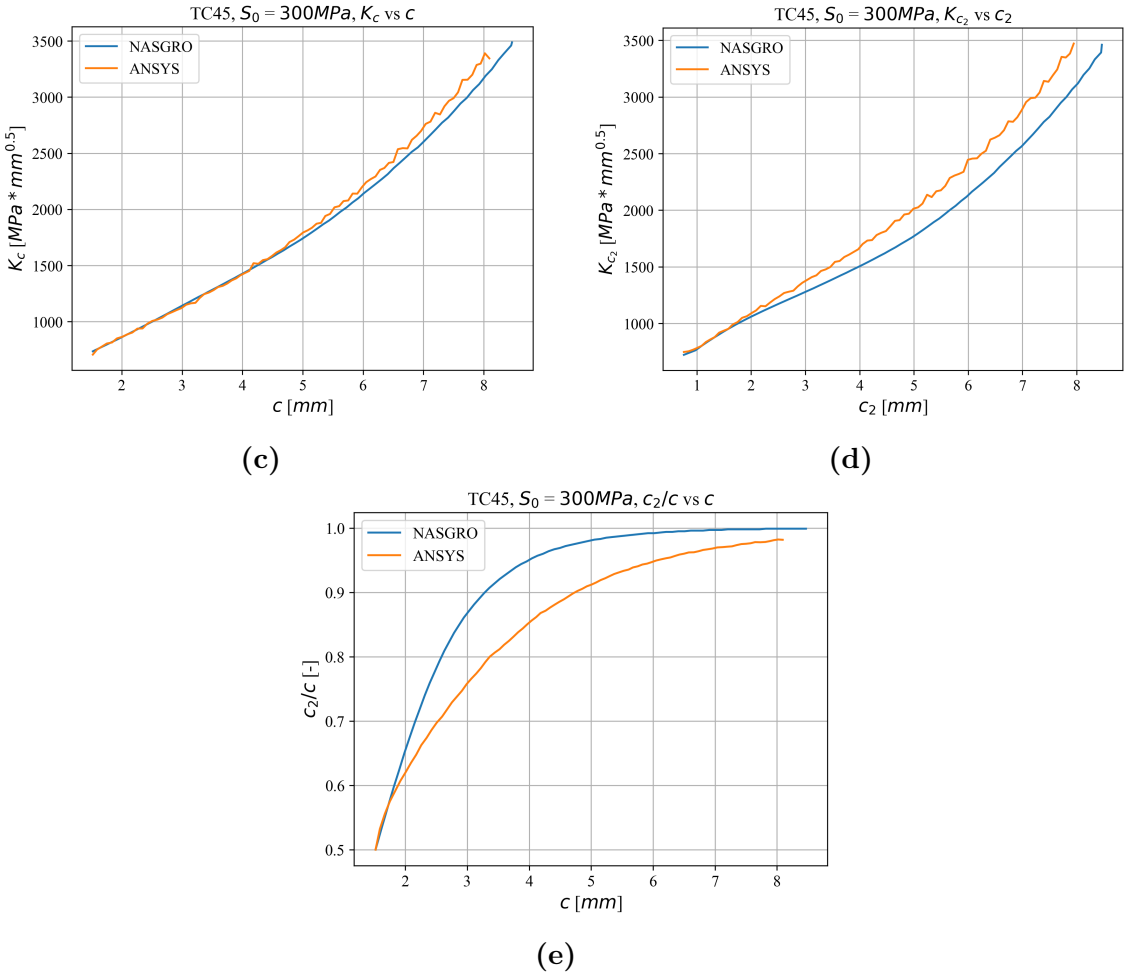

Figure 4.6: Comparison between NASGRO and ANSYS, for TC45 with $S_0 = 300\,\text{MPa}$, $R = 0$ loading. **(a)**: c vs N. **(b)**: c_2 vs N. **(c)**: K_c vs c. **(d)**: K_{c_2} vs c_2. **(e)**: c_2/c vs c.

For the TC45 crack configuration subjected to S_0 loading, the results show good agreement between NASGRO and ANSYS in terms of SIFs, crack length evolution, and final predicted number of load cycles, with NASGRO yielding a slightly more conservative life-time prediction.

The results also indicate the presence of oscillations in the SIF values obtained from ANSYS. This observation is consistent with the results obtained for through-crack configurations. The observed behaviour may be attributed to discontinuities introduced during the remeshing process.

The results for bending loading, $S_1 = 400\,\text{MPa}$, $R = 0$, are shown in Figure 4.7.

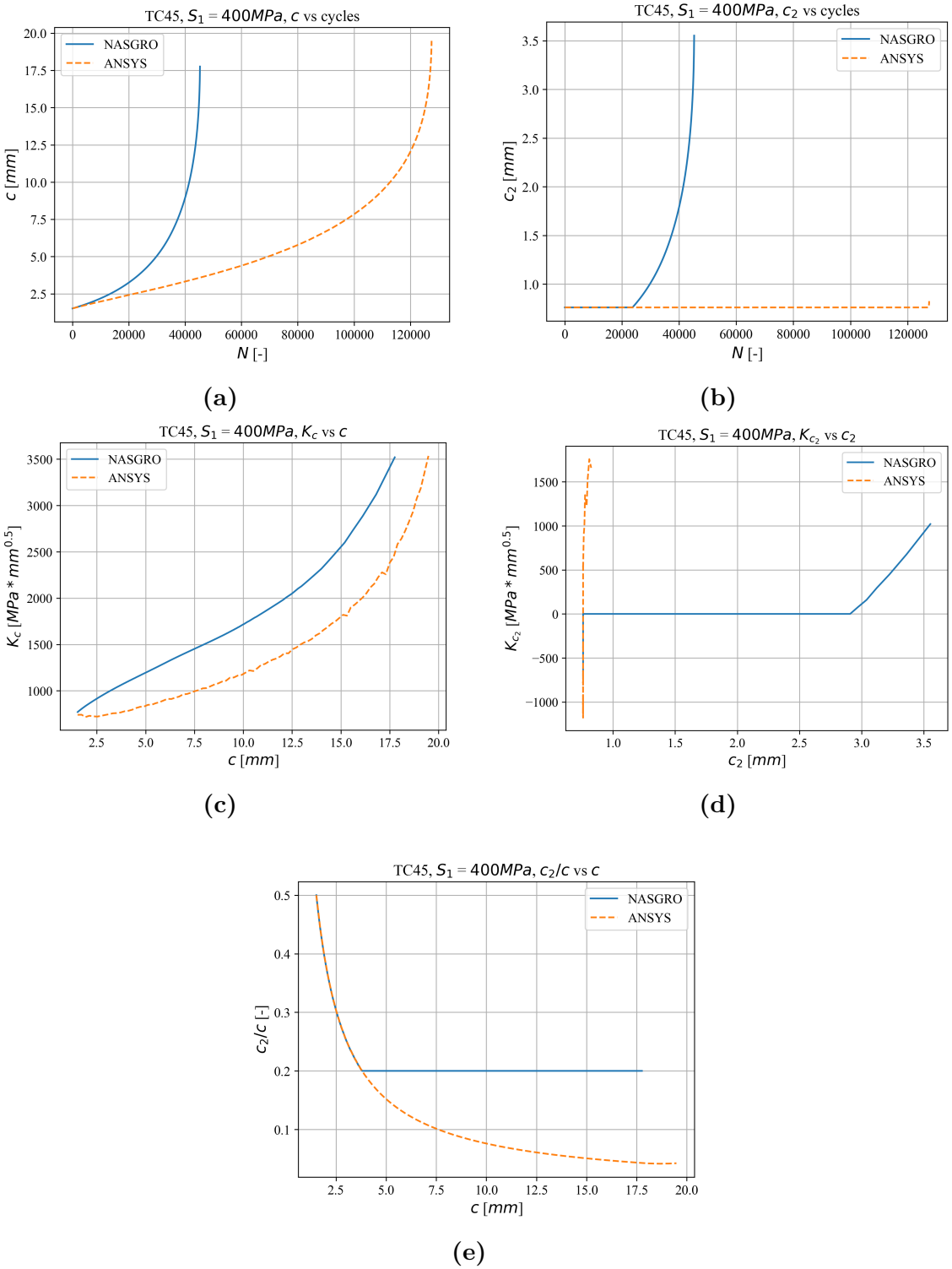

Figure 4.7: Comparison between NASGRO and ANSYS, for TC45 with $S_1 = 400\,\text{MPa}$, $R = 0$ loading. **(a)**: c vs N. **(b)**: c_2 vs N. **(c)**: K_c vs c. **(d)**: K_{c_2} vs c_2. **(e)**: c_2/c vs c.

A pronounced difference in conservativeness is observed for the TC45 geometry un-

der S_1 bending. For this configuration, ANSYS predicts a shorter life-time than NASGRO and can therefore be regarded as the more conservative approach. The observed discrepancy is largely attributed to modelling assumptions implemented in NASGRO, which influence the crack growth behaviour under this loading condition.

Compressive loading is present at the c_2 node for the TC45 configuration under through-thickness bending. Figure 4.7(b) shows that no crack growth occurs initially at the c_2 node until approximately 25 000 cycles, after which NASGRO predicts a rapid increase in crack length. As shown in Figure 4.7(d), this behaviour is not caused by crack opening leading to a positive SIF, but rather by a geometrical constraint in NASGRO requiring that $c_2 \geq 0.2c$. This is confirmed by the aspect ratio evolution shown in Figure 4.7(e).

As a result, the c_2 dimension is artificially increased, which significantly alters the crack-front geometry and affects subsequent crack growth behaviour. This forced crack growth leads to earlier predicted failure and may therefore introduce a conservative bias in the results. In contrast, ANSYS does not impose such geometrical constraints, resulting in no forced growth at the c_2 node. However, as shown in Figures 4.7(b) and 4.7(d), some crack opening and growth at the c_2 node is still observed in ANSYS at later stages of the simulation. This is evidenced by the transition from negative to positive SIF values at the c_2-node in Figure 4.7(d). This behaviour is expected, as the entire crack front tends to open when the crack size becomes large. At this stage, the crack geometry approaches that of a straight through crack near the specimen edge.

The less constrained model in ANSYS resulted in limited growth at the c_2-node, leading to the development of a longer and therefore numerically more complex crack front, see Figure 4.8. The crack front illustration shows that no crack growth occurs at the c_2-node, leading to a markedly elongated crack front. The increased crack-front complexity contributed to remeshing difficulties, which necessitated adjustments to both the crack front element size and the maximum incremental crack extension. As described in Section 3.3.1, such changes can provide inaccurate life-time predictions.

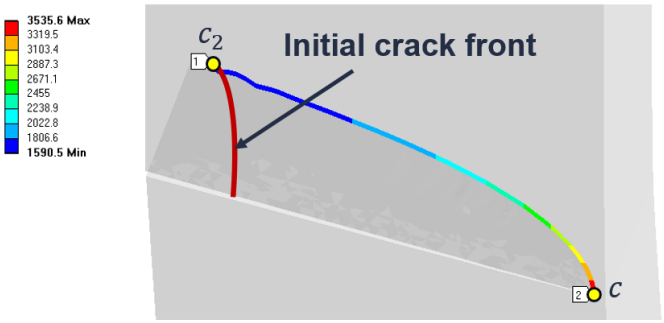

Figure 4.8: Crack front shape and SIFs at the point of fracture for TC45 in ANSYS, with bending loading $S_1 = 400\,\text{MPa}$ and stress ratio $R = 0$.

The results for in-plane bending loading, $S_2 = 300\,\text{MPa}$, $R = 0$, are shown in Figure

4.9.

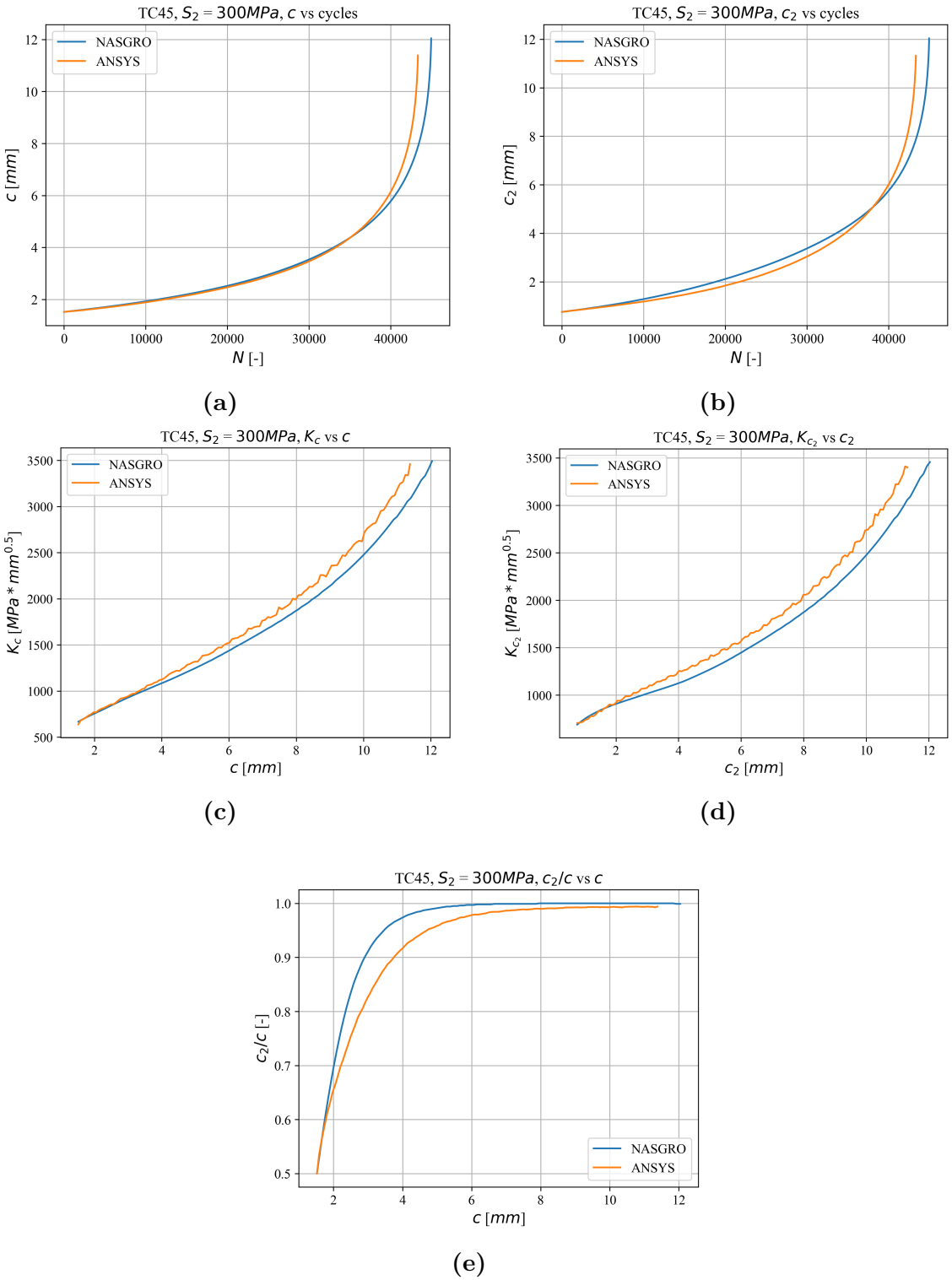

Figure 4.9: Comparison between NASGRO and ANSYS, for TC45 with $S_2 = 300\,\text{MPa}$, $R = 0$ loading. **(a)**: c vs N. **(b)**: c_2 vs N. **(c)**: K_c vs c. **(d)**: K_{c_2} vs c_2. **(e)**: c_2/c vs c.

For the TC45 crack configuration subjected to S_2 loading, the results show good agreement between NASGRO and ANSYS in terms of SIFs, crack length evolution, and final predicted number of load cycles, with ANSYS yielding a slightly more conservative life-time prediction. The crack growth plots exhibit an intersection between the predictions from the two software packages at approximately 37 000 cycles, which is particularly evident in Figure 4.9(b). This behaviour may be attributed to the change in slope of the SIF evolution observed in the ANSYS results at a crack extension of approximately 2 mm, as shown in Figure 4.9(d). The results also indicate the presence of oscillations in the SIF values obtained from ANSYS which may be attributed to mesh discontinuities.

4.4 Effects of stress ratio

In this section, results regarding the effects of changing the stress ratio to $R = -1$ will be presented. First, a comparative example of CC09 subjected to a tensile loading of $S_0 = 300$ MPa for $R = 0$ and $R = -1$ is presented to illustrate the effect on the crack growth rate. This is followed by analyses of CC09 and TC45 subjected to through-thickness bending $S_1 = 300$ MPa and $R = -1$ to illustrate the effect of non-uniform crack opening. In ANSYS, reversed loading conditions were implemented using the CLOAD command, and the effective SIF range was evaluated using the mode-separation method (CGROW, NPLOAD, METH, DKMOD).

Figure 4.10 presents crack growth versus cycles and SIFs versus crack extension for the CC09 configuration subjected to fully reversed tensile loading. Corresponding results for purely tensile loading ($R = 0$) are also included for comparison.

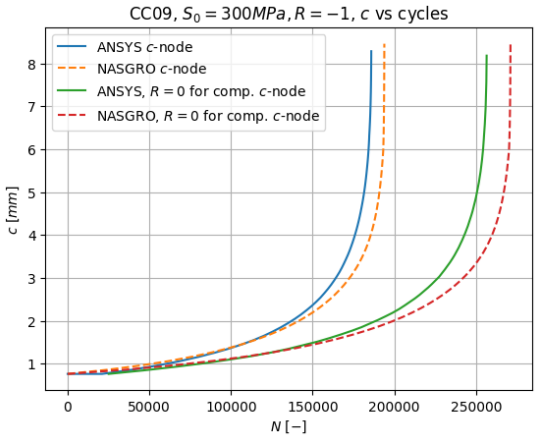

(a)

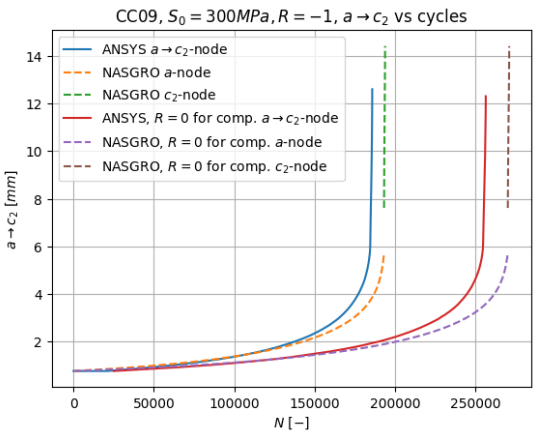

(b)

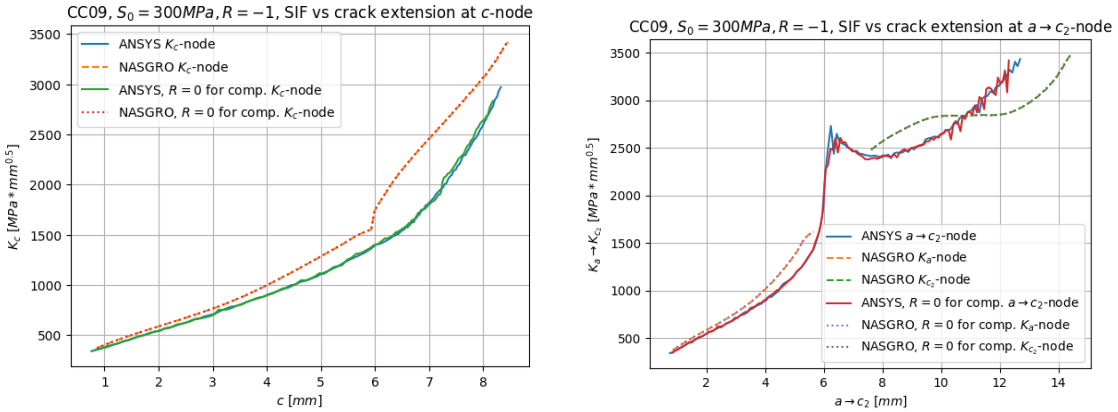

(c) **(d)**

Figure 4.10: Comparison between NASGRO and ANSYS for CC09 with $S_0 = 300\,\text{MPa}$ and $R = -1$ loading. Solutions for CC09 $S_0 = 300\,\text{MPa}$ $R = 0$ also included for reference. **(a)**: c vs N. **(b)**: c_2 vs N. **(c)**: K_c vs c. **(d)**: K_{c_2} vs c_2.

The results show that, for the tensile loading case, the two tools exhibit good agreement. It is also observed that a fully reversed loading condition results in higher crack growth rates and, consequently, shorter fatigue lives.

Figure 4.11 presents the corresponding results for CC09 subjected to fully reversed through-thickness bending. The ANSYS simulations were terminated earlier due to remeshing limitations; however, the results provide sufficient information for comparison.

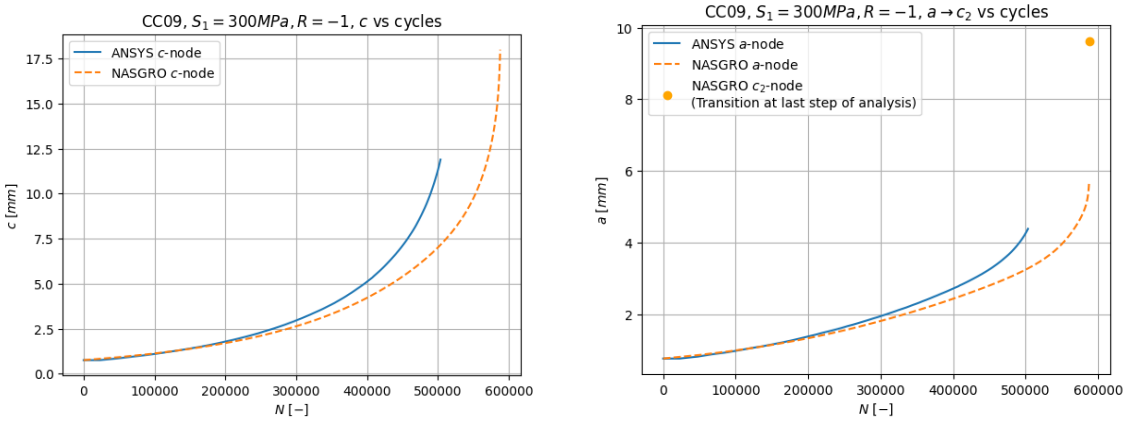

(a) **(b)**

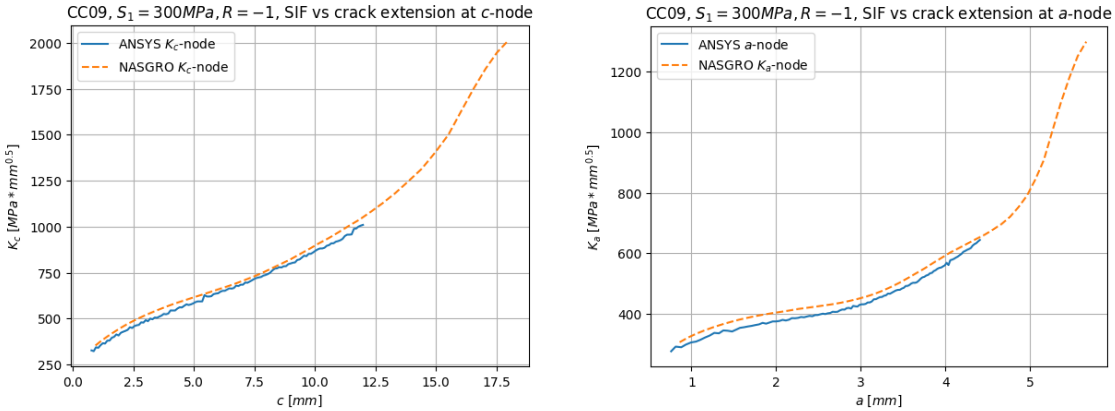

(c) **(d)**

Figure 4.11: Comparison between NASGRO and ANSYS for CC09 with $S_1 = 300\,\text{MPa}$ and $R = -1$ loading. **(a)**: c vs N. **(b)**: a vs N. **(c)**: K_c vs c. **(d)**: K_a vs a.

The results show good agreement for the fully reversed through-thickness bending case, with ANSYS predicting slightly more conservative crack growth rates. A key difference is that NASGRO predicted crack transition right before the analysis was terminated due to geometrical constraints.

Figure 4.12 presents the crack shape, crack growth over cycles, and SIF evolution with crack extension for the TC45 configuration subjected to fully reversed through-thickness bending. As in the previous case, the ANSYS simulations were terminated earlier due to remeshing limitations; however, they still provide sufficient data for comparison.

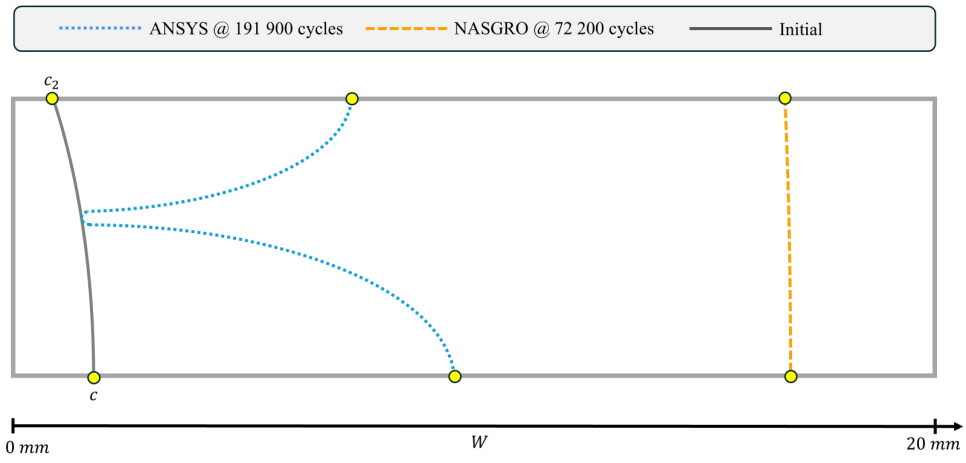

(a)

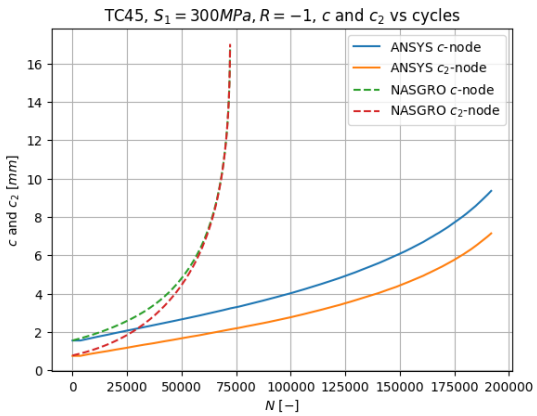

(b)

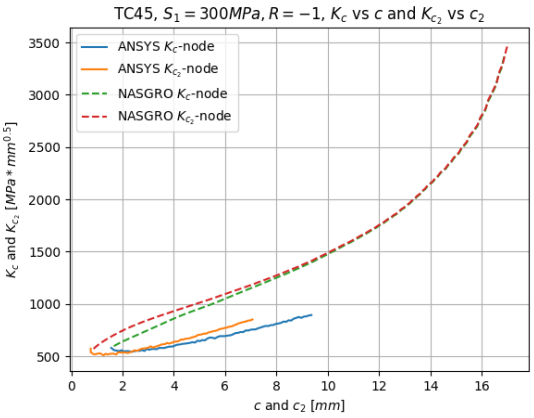

(c)

Figure 4.12: Comparison between NASGRO and ANSYS for TC45 with $S_1 = 300\,\text{MPa}$ and $R = -1$ loading.**(a)**: Crack shape after certain amount of cycles. **(b)**: Crack extensions at c and c_2 node vs cycles. **(c)**: K_c vs c and K_{c_2} vs c_2.

For the TC45 configuration, pronounced differences between ANSYS and NASGRO are observed. These differences are primarily associated with variations in crack-front geometry, as illustrated in Figure 4.12(a), which directly influence the computed SIF values and the resulting crack growth rates.

Under fully reversed bending, the crack front experiences non-uniform loading conditions, where different regions are subjected to tensile, compressive, or negligible loading during different phases of the cycle. This non-uniform crack opening behaviour is clearly reflected in the ANSYS results.

To capture this behaviour, ANSYS requires explicit modelling of reversed loading using the CLOAD and NPLOAD commands. In contrast, NASGRO provides a simplified representation of the loading, resulting in a more straightforward implementation.

However, NASGRO represents the crack front using a limited number of evaluation points, see Section 3.2.1, and assumes uniform crack growth between these points. This assumption limits its ability to capture non-uniform crack-front behaviour. In the present case, ANSYS captures the existence of a non-stressed location (neutral axis under bending), within the thickness, where no crack growth occurs. This behaviour is reflected in the crack-front shape shown in Figure 4.12(a), resulting in a crack-front evolution that may be more representative of the physical response.

4.5 Quarter-elliptical corner crack at hole in lug (CC19)

This section presents the results obtained for the lug geometry with a quarter-elliptical corner crack, corresponding to the CC19 crack case. The simulations were

performed under pin-loading for load ratios of $R = 0$ and $R = -1$. In addition to the crack propagation results, this section also includes the load application investigation described in Section 3.1.2.1, which was conducted to assess the influence of load definition on the numerical predictions. The results for $R = 0$ are shown in Figure 4.13.

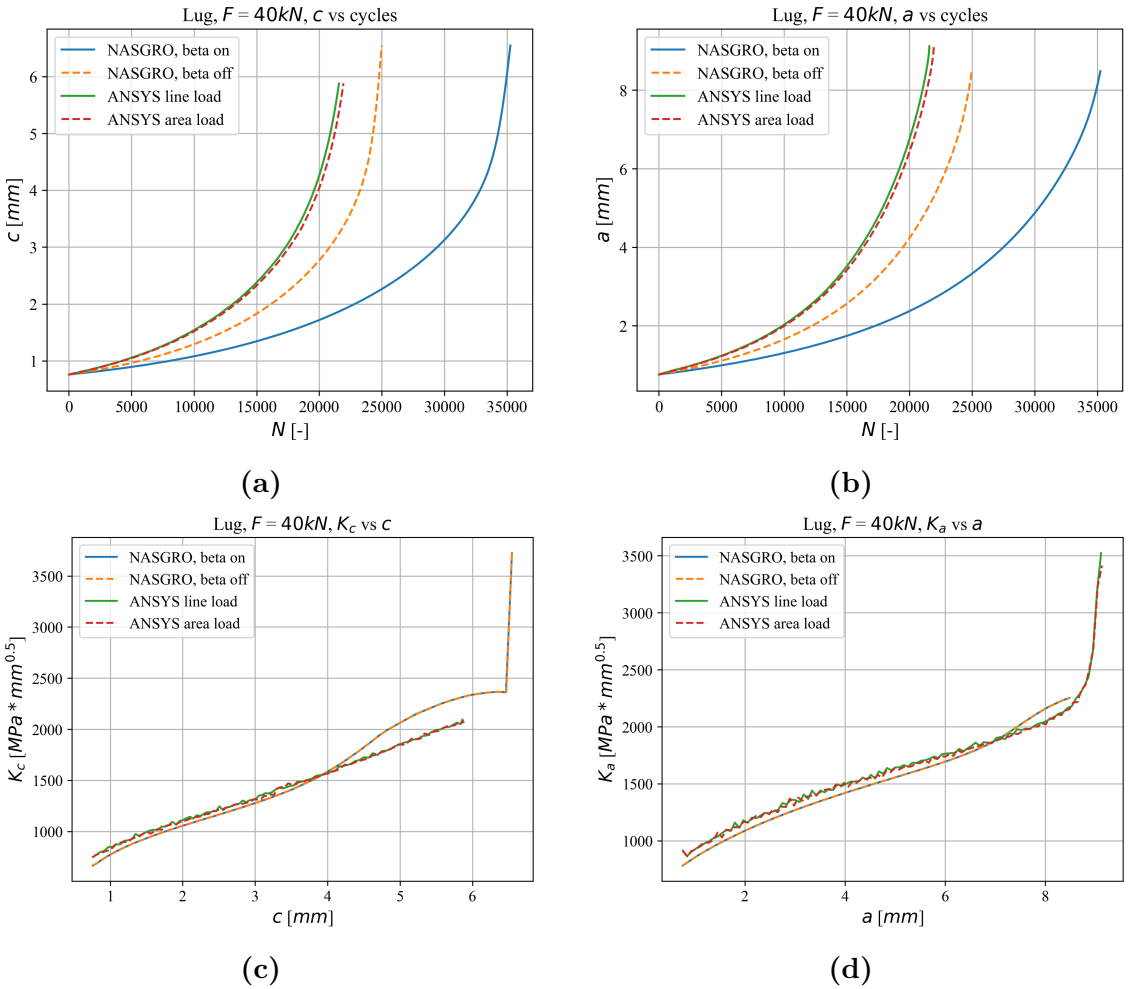

Figure 4.13: Comparison between NASGRO and ANSYS, for CC19 with $F = 40\,\text{kN}$ loading. **(a)**: c vs N. **(b)**: a vs N. **(c)**: K_c vs c. **(d)**: K_a vs a.

For the lug geometry subjected to tensile loading with load ratio $R = 0$, the results indicate pronounced discrepancy between the two software packages. The area and line load cases in ANSYS achieved similar results for both SIFs and crack length evolution. For further analyses, the line load application was used due to simpler implementation. Turning the β-factor off in NASGRO resulted in more similar results to ANSYS. On the other hand, in NASGRO, multiplying ΔK with the β-factor is said to produce a more accurate crack growth prediction [4]. Note that CC19 in NASGRO offers only transition to a straight through crack. This can be seen through the sudden increase in K_c values after which the fracture toughness is exceeded.

In addition, a crack growth rate comparison for the $R = 0$ simulation is shown in Figure 4.14.

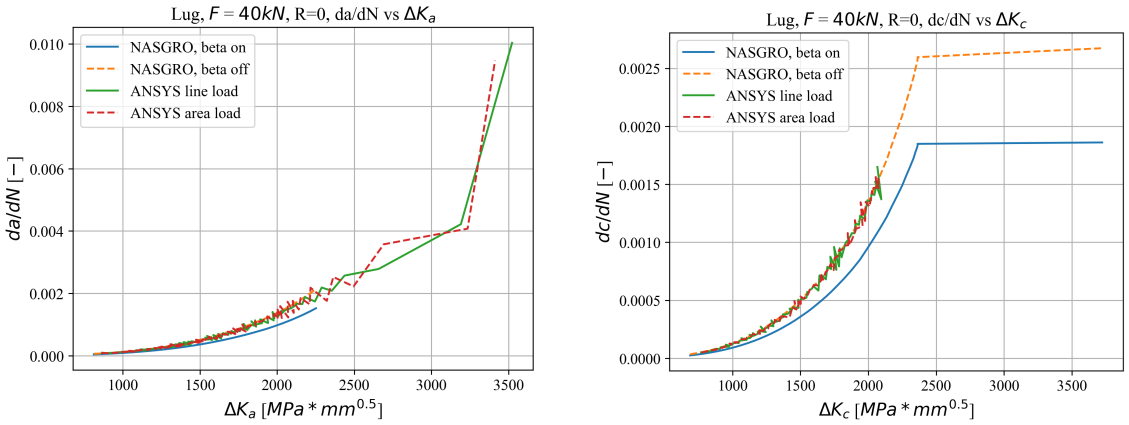

(a) **(b)**

Figure 4.14: Results of crack growth rate da/dN and dc/dN vs ΔK_a and ΔK_c for respective simulation done for CC19. **(a)**: da/dN vs ΔK_a. **(b)**: dc/dN vs ΔK_c.

As shown in Figure 4.14, improved agreement between ANSYS and NASGRO is obtained when the β-factor in NASGRO is disabled.

The results for the lug with $R = -1$ are shown in Figure 4.15. The results obtained with and without compression clipping, both with and without the inclusion of the β-factor, are compared against the ANSYS simulation.

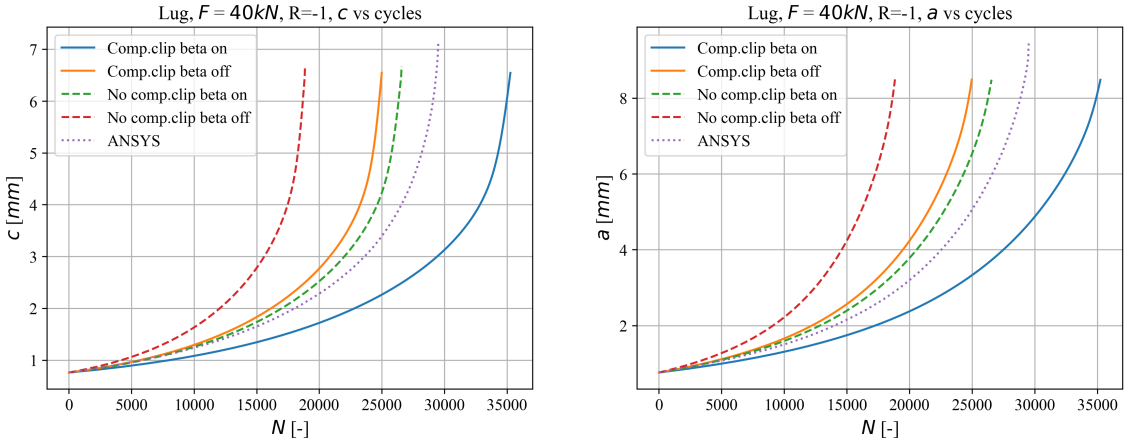

(a) **(b)**

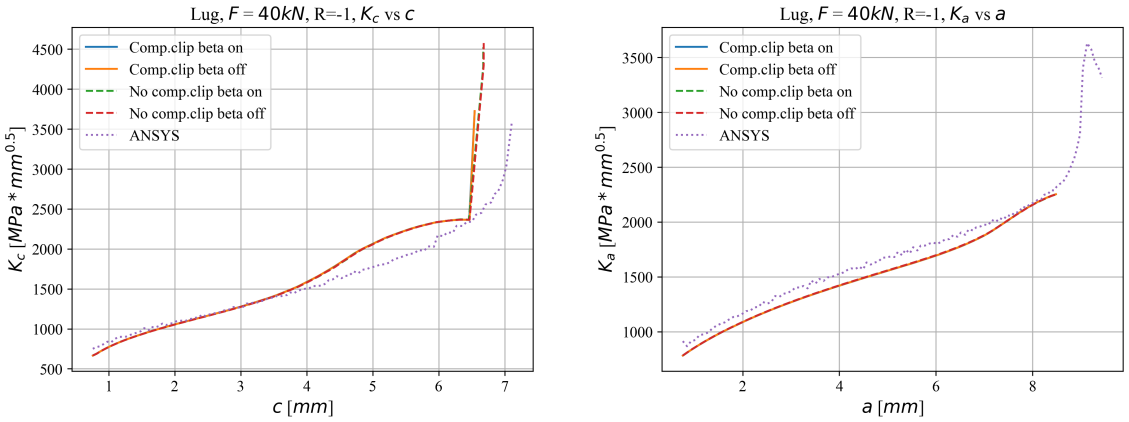

(c) **(d)**

Figure 4.15: Comparison between NASGRO and ANSYS, for CC19 with $F = 40\,\text{kN}$ loading, and $R = -1$. **(a)**: c vs N. **(b)**: a vs N. **(c)**: K_c vs c. **(d)**: K_a vs a.

For the lug geometry, the results obtained for a load ratio of $R = -1$ indicate that the NASGRO solution employing compression clipping yields results equivalent to those predicted for $R = 0$. This effect arises from considering only the positive portion of the loading cycle, wherein negative K values are set to zero [28]. In contrast, the ANSYS results for $R = -1$ exhibit more pronounced deviations compared to the corresponding $R = 0$ case. Furthermore, not including compression clipping in NASGRO yields in more conservative results predicting shorter life-time. This is expected since NASGRO is treating the negative portion of the loading cycle as proportional loading. Consequently, a noticeable discrepancy between the two software packages is observed for this loading condition.

ANSYS implements the negative load ratio by alternating the applied load between the upper and lower regions of the hole, using the NPLOAD method (CGROW, NPLOAD, METH, DKMOD) as described in Section 3.3.2. This approach provides a higher level of numerical consistency with the physical problem, as the actual loading scenario involves a pin transferring contact forces between opposing sides of the hole.

In addition, it can be observed that crack transition to a through crack occurs for both stress ratio cases in NASGRO, and for the $R = -1$ case in ANSYS. This behaviour is evident from the SIF plots, which exhibit abrupt increases or decreases depending on which crack-front node propagates to the free surface. As previously discussed, deviations exist in how the two software packages define and handle crack transition. These differences in transition treatment provide a plausible explanation for the discrepancies observed between the NASGRO and ANSYS results following crack transition.

Nevertheless, compressive and tensile effects on the crack still occurs when the load is applied to the lower region of the hole resulting in a non-uniform crack front behaviour, meaning that there is no constant crack opening or crack closure along the

front. Since the ANSYS results remain within a reasonable range when compared to those obtained from NASGRO, it can be inferred that the contribution of SIFs during load at the bottom of the hole has a limited influence on the overall crack growth behaviour. This observation is supported by the results presented in Figure 4.16, which shows the relatively low SIFs compared to the maximum value in the top nodes loading part.

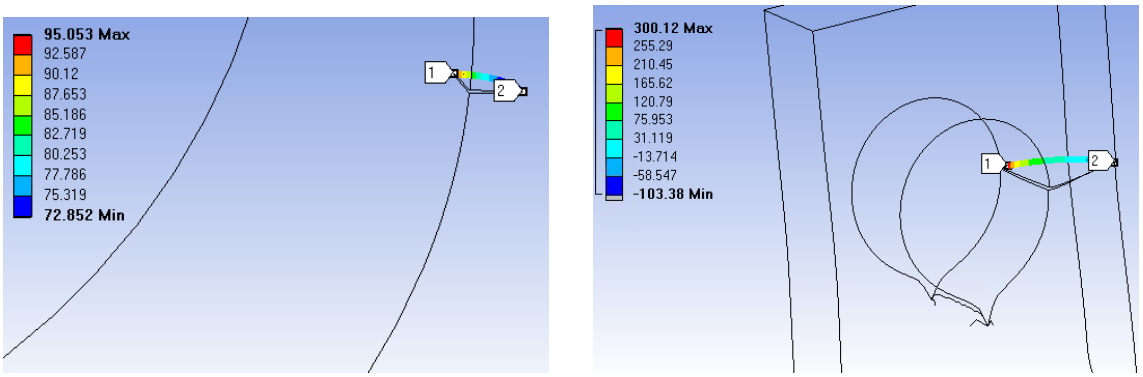

(a) **(b)**

Figure 4.16: CC19 subjected to fully reversed load. SIF contour at crack front during **(a)**: first compressive load cycle **(b)**: last compressive load cycle.

The results presented in Figure 4.16 show both negative and positive SIF values during the compression phase of the loading cycle in ANSYS, for both the initial and final load cycles. This indicates that the crack experiences both opening and closure during this portion of the cycle. Consequently, it suggests that applying compression clipping alone may not be sufficient to accurately represent the compression phase, as this part of the loading cycle still contributes to crack growth behaviour.

However, it is also evident from Figure 4.16 that the SIF magnitudes in this region are relatively small compared to those shown in Figures 4.15(c) and 4.15(d), which may imply a limited overall contribution. The investigation of the β-factor further revealed that it is not accounted for in ANSYS.

Moreover, as illustrated in Figures 4.15(a) and 4.15(b), the results obtained from ANSYS and NASGRO show better agreement when compression clipping is applied with the β-factor disabled, compared to the case without compression clipping and with β turned off. This suggests that incorporating compression clipping yields behaviour more consistent with ANSYS simulations. Nevertheless, completely eliminating negative SIF values may not be entirely appropriate, as the compression phase still exerts some influence on crack propagation.

5
Discussion

This chapter discusses the main findings of the study with respect to crack growth behaviour, fatigue life predictions, and differences between the ANSYS and NASGRO software tools. The results presented in Chapter 4 are interpreted in terms of modelling approaches, numerical implementation, and underlying assumptions.

Particular emphasis is placed on differences in SIF evaluation, crack transition modelling, and the treatment of compressive loading effects. The implications of these differences for accuracy, computational efficiency, and applicability in engineering practice are also considered. Finally, key sources of uncertainty and limitations in the comparative analysis are discussed.

5.1 Life-time predictions

Fatigue life predictions vary systematically with crack configuration, loading type, and stress ratio. Across all investigated cases, no consistent trend was observed indicating that one tool is uniformly conservative. Instead, the relative conservativeness depends on the underlying crack-front behaviour and modelling assumptions associated with each configuration.

For cases involving relatively uniform crack-front evolution (for example under purely tensile loading), both ANSYS and NASGRO produce comparable fatigue life predictions. In these cases, the SIF distributions are similar and crack growth proceeds in a consistent manner, indicating that both approaches capture the dominant crack driving forces.

However, significant differences in fatigue life arise when non-uniform crack-front behaviour (such as under bending load) or geometric constraints become dominant. A representative example is the TC45 configuration under bending, where NASGRO enforces the geometrical constraint $c_2/c \geq 0.2$. This constraint drives crack growth at the back-face node independently of the local SIF state, resulting in an increased crack length and elevated SIF values, see Figure 4.7. Consequently, crack growth is accelerated and fatigue life is reduced. In contrast, ANSYS allows the crack front to evolve freely, leading to delayed growth at the back face and a different crack-front shape. This highlights that geometrical constraints can directly influence fatigue life predictions through their impact on crack-front evolution.

5.2 Transition modelling

Crack transition is identified as a primary source of discrepancy between ANSYS and NASGRO. In NASGRO, transitions are modelled by predefined criteria and are accompanied by instantaneous changes in crack geometry. This introduces discontinuities in both crack-front shape and SIF distribution at the transition point.

For SC30 and CC19, the transition to a straight through crack imposes a uniform crack-front definition, as shown in Figure 5.1. This results in an abrupt increase in SIF values, as the entire crack front suddenly adopts the maximum crack depth. Consequently, the crack growth rate increases rapidly, and failure occurs shortly after transition. This behaviour was consistently observed in the results as pronounced jumps in both crack length and SIF values.

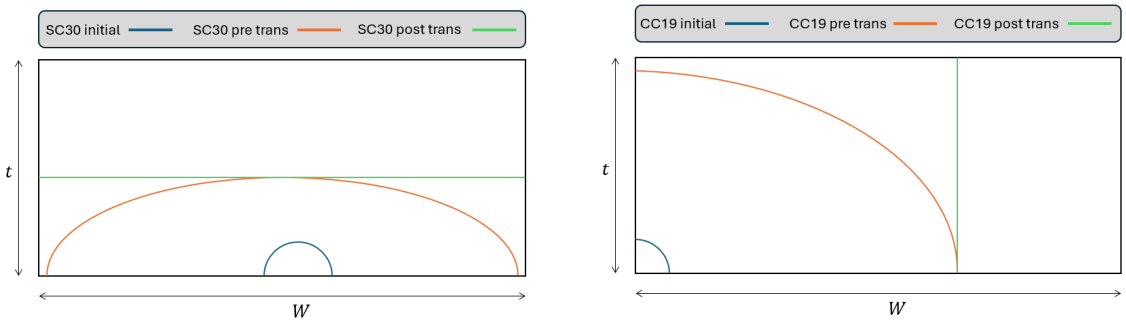

(a) **(b)**

Figure 5.1: Transition to a straight through crack for **(a)**: SC30, and **(b)**: CC19.

In contrast, CC09 transitions to a curved through crack (TC45), resulting in a smaller geometric discrepancy and a more gradual change in crack-front conditions. As a result, the post-transition behaviour shows improved agreement with ANSYS.

In ANSYS, no predefined transition geometry is imposed. Instead, the crack front evolves continuously, leading to smoother transitions in both geometry and SIF. As shown, the SIF value at the transition node undergoes a rapid increase after which the SIF drops which is consistent with theory, see Section 2.3.3.

An additional crack formulation that could provide a more physically realistic representation of the transition process would be the introduction of a through-crack model defined by three computational points along the crack front, for example corresponding to a, c, and c_2. Such a representation would allow for a gradual redistribution of crack-front geometry during transition, rather than the instantaneous adoption of a simplified configuration.

In the case of SC30, a three-point post-transition model would enable the crack to retain information about its pre-transition shape, allowing different regions of the crack front to evolve at different rates. This concept is illustrated in Figure 5.2. Compared to the current straight through-crack formulation, this would reduce the

abrupt changes in SIF observed at transition and enable a more continuous evolution of both crack geometry and crack growth rate.

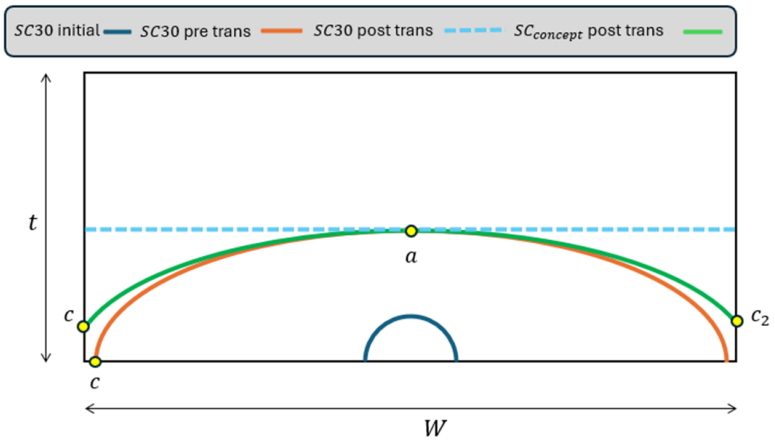

Figure 5.2: Conceptual post-crack configuration for SC30 with three computational points.

Such a formulation would bridge the gap between the simplified NASGRO representation and the fully resolved crack-front modelling in ANSYS. It would provide increased flexibility in representing non-uniform crack-front behaviour while maintaining a relatively low computational cost compared to full finite element simulations. This type of intermediate modelling capability could therefore significantly improve the accuracy of transition predictions within NASGRO without compromising its efficiency.

Overall, the results demonstrate that the definition of post-transition geometry is a governing factor for crack growth behaviour. When the imposed geometry differs significantly from the pre-transition crack shape, large discrepancies between the two tools arise.

For all investigated cases in ANSYS involving a through crack, oscillations are observed in the obtained SIF values. This behaviour may be attributed to numerical discontinuities introduced during the remeshing process.

5.3 Effects of compressive loads on the crack front

For simple loading conditions, such as tensile loading, both ANSYS and NASGRO show good agreement. In these cases, crack opening occurs only during the tensile portion of the cycle, and the effective SIF range is governed primarily by $K_{\max}$. This results in consistent predictions of increased crack growth rates and reduced fatigue life for $R = -1$.

In contrast, for through-thickness bending, the crack front is subjected to spatially

varying loading conditions, where different regions experience alternating tension and compression. This leads to non-uniform crack opening along the crack front. ANSYS captures this behaviour explicitly when reversed loading is applied using CLOAD, allowing the crack front to respond locally to the applied stress state. In this case, regions under compression exhibit limited or no crack growth, resulting in an elongated crack front with a distinct no-growth point, see Figure 4.12.

These differences demonstrate that the treatment of compressive loading is critical in cases involving non-uniform crack opening, and that simplified approaches may not fully capture the local crack-front response.

5.4 Sources of error

A comparative study of two different software tools inherently includes several potential sources of error that may influence the results. In addition to the limitations outlined in Section 1.3, such as the assumptions of LEFM and Mode I loading, this section highlights further sources of uncertainty that may have affected the comparison.

One fundamental difference between the software tools lies in the calculation of SIFs. NASGRO evaluates SIFs using parameterised expressions based on a large set of reference solutions, whereas ANSYS computes SIFs directly using the interaction integral method. The ANSYS simulations are also highly dependent on mesh quality and other sensitivity-related parameters. Due to computational constraints, mesh refinement had to be balanced against simulation time, which may have affected the accuracy of the results. Additionally, the presence of non-uniform behaviour, such as compressive loading, reduced mesh quality and in some cases led to premature termination of the simulations, thereby introducing additional uncertainty into the results.

Furthermore, NASGRO evaluates crack growth at a limited number of points along the crack front. While this approach is sufficient for simpler crack configurations, it may not provide adequate resolution for more complex cases involving non-uniform crack-front behaviour. In addition, crack transitions in NASGRO are handled using predefined algorithms, which may influence the evolution of the crack geometry after transition and do not fully capture the physical transition behaviour.

The observed differences between ANSYS and NASGRO can therefore be attributed to a combination of modelling assumptions, numerical implementation strategies, and software-specific limitations, particularly with respect to crack-front resolution, transition modelling, and the treatment of compressive loading.

6
Conclusion

This thesis presented a comparative study of fatigue crack growth predictions using the ANSYS SMART FE framework and the NASGRO analysis tool. The results demonstrate that there is no universally superior approach; rather, the suitability of each tool depends strongly on the specific crack configuration, loading conditions, and desired level of accuracy.

The following conclusions can be drawn from the comparative study of ANSYS and NASGRO for fatigue crack growth analysis:

- For configurations with uniform crack-front behaviour, both tools provide comparable SIF predictions and fatigue life estimates, indicating that simplified approaches are sufficient in this regime.
- Differences in fatigue life predictions arise primarily in cases involving transitions and non-uniform crack-front behaviour; such as through-thickness bending and fully reversed loading.
- NASGRO enforces geometrical constraints and predefined transition geometries, which can drive crack growth independently of local SIF conditions, leading to accelerated crack propagation and reduced fatigue life.
- Crack transition modelling is a major source of discrepancy. Abrupt changes in crack geometry in NASGRO lead to sudden increases in SIF values, whereas ANSYS allows continuous crack-front evolution.
- ANSYS provides a higher-fidelity representation of crack-front behaviour and is capable of capturing non-uniform crack growth and local equilibrium conditions. However, this comes at the cost of increased computational effort and sensitivity to mesh quality. ANSYS can take up to days for one single simulation, while NASGRO finishes the simulation within seconds.
- NASGRO offers a computationally efficient and robust approach for standard fatigue analyses, requiring significantly less preprocessing and user interaction compared to finite element modelling. This makes it more accessible and user-friendly for engineering applications, although it is limited in its ability to resolve complex crack-front behaviour and transition phenomena.
- The two tools should be regarded as complementary: NASGRO is suitable for rapid engineering assessments, while ANSYS is better suited for detailed analyses of complex loading and crack geometries.

In addition, the investigations in the current work led to following observations.

NASGRO v.11.1:

1. Crack type SC30 in NASGRO allows transition to a curved through crack. But this is only applicable when the interior tip (a-tip) reaches the thickness boundary. If the surface tip (c-tip) reaches the width boundary, the post-transition crack has a straight crack front.

2. A curved through crack in NASGRO is represented by two tips at the two ends (where the crack front intersects with free surface). Consequently, such a crack cannot capture a tunnelling behaviour where the interior part of the crack front grows differently than the parts close to the two free surfaces.

ANSYS Workbench 2024 R1/2025 R2:

1. A converged result is obtained when the crack front element size is about one-fifteenth of the initial crack size. The fatigue results are less sensitive to the crack growth increment size. One-fifteenth of the initial crack size provided reasonably accurate results.

2. A growing crack in through crack geometries often lead to oscillatory behaviour in stress intensity factor along the crack front. This is possibly due to somewhat unstructured crack front mesh in this case (compared to surface and corner cracks). The oscillatory behaviour shows up even when a surface crack or a corner crack transitions to a through crack.

3. Simulation of crack growth under non-proportional loads and fully reversed loads require explicit modelling of all load steps, through commands such as CLOAD and CGROW, NPLOAD, METHOD, DKMOD

6.1 Future work recommendations

Future work should include validation of the numerical results against experimental fatigue crack growth data in order to quantify the predictive accuracy of both approaches and assess their applicability in real-world engineering scenarios.

Further improvements in mesh generation and remeshing strategies in ANSYS are recommended, as these would increase robustness and reduce the occurrence of premature simulation termination, particularly for complex crack-front geometries.

In addition, the present study could be extended to more complex structural components and multi-axial loading conditions to better reflect realistic engineering applications. Such investigations would provide further insight into the limitations and capabilities of both tools under practical operating conditions.

Bibliography

[1] Jia Hui Lv et al. "Failure Cases Analysis in Aerospace Field". In: *Materials Science Forum* 993 (2020), pp. 1277–1285. ISSN: 1662-9752. DOI: 10.1016/S0142-1123(03)00145-2.

[2] Selim Gürgen. *Failure in Aircraft Materials*. Springer Nature Switzerland AG, 2025.

[3] S. M. O. Tavares and P. M. S. T. De Castro. "An overview of fatigue in aircraft structures". In: *Fatige Fracture of Engineering Materials Structures* 40 (10 2017), pp. 1510–1529. DOI: 10.1111/ffe.12631.

[4] Southwest Research Institute. *NASGRO® Fracture Mechanics And Fatigue Crack Growth Analysis Software*. Version 11.1. 2025.

[5] Tianyu He et al. "Strategy for simulating high-speed crack propagation in 3D-plate structures based on S-version FEM". In: *International Journal of Mechanical Sciences* 274 (2024), pp. 1510–1529. DOI: 10.1016/j.ijmecsci.2024.109261.

[6] Ansys Inc. *Fracture Analysis Guide*. 2025. URL: https://ansyshelp.ansys.com/public/Views/Secured/corp/v251/en/pdf/Ansys_Mechanical_APDL_Fracture_Analysis_Guide.pdf.

[7] FEAmax LLC Engineering Services. *Ensuring Structural Integrity with FEA Crack Propagation Analysis*. Accessed: 2026-01-22. URL: https://www.feamax.com/crack-propagation-analysis-on-engine-model/#:~:text=Performing%20FEA%20Crack%20Propagation%20Analysis%20is%20essential,performance%20and%20safety%20over%20the%20component%27s%20lifespan..

[8] Southwest Research Institute. *NASGRO® Fracture Mechanics Fatigue Crack Growth Software*. Accessed: 2026-01-22. URL: https://www.swri.org/markets/chemistry-materials/materials/mechanics-materials/nasgro-fracture-mechanics-fatigue-crack-growth-software.

[9] P. Paris, M. Gomez, and W. Anderson. "A rational analytic theory of fatigue". In: *The trend in Engineering* 13 (1961), pp. 9–14.

[10] K Walker. "The Effect of Stress Ratio During Crack Propagation and Fatigue for 2024-T3 and 7075-T6 Aluminum". In: *Effects of Environment and Complex Load History on Fatigue Life* STP462-EB (1970). DOI: https://doi.org/10.1520/STP32032S.

[11] R. G: Forman, V. E. Kearney, and R. M. Engle. "Numerical Analysis of Crack Propagation in Cyclic-Loaded Structures". In: *Journal of Basic Engineering* 83 (3 1967), pp. 459–463. DOI: https://doi.org/10.1115/1.3609637.

[12] B. Moreno et al. "Estimations of fatigue life and variability under random loading in aluminum Al-2024T351 using strip yield models from NASGRO".

In: *International Journal of Fatigue* 91 (2016), pp. 414–422. DOI: https://doi.org/10.1016/j.ijfatigue.2015.09.031.

[13] F. Elfving and J. Hæg. "Potentials and limitations in finite element based crack propagation analysis using FRANC3D". MA thesis. Chalmers University of Technology, 2020.

[14] Inc Fracture Analysis Consultants. *FRANC3D User's Guide*. Version 9.0. 2026.

[15] Ted L. Anderson. *Fracture Mechanics: Fundamentals and Applications*. 3rd ed. Boca Ranton, FL, USA: CRC Press, 2005.

[16] Wikimedia Commons. *File:Crack-tip-stress-field.svg*. Accessed on: 2026-02-13. 2025. URL: https://commons.wikimedia.org/wiki/File:Crack-tip-stress-field.svg.

[17] Wikimedia Commons. *File: Fracture modes v2.svg*. Accessed on: 2026-01-26. 2014. URL: https://commons.wikimedia.org/w/index.php?title=File:Fracture_modes_v2.svg&oldid=142763665.

[18] Norman E. Dowling. *Mechanical behavior of materials: engineering methods for deformation, fracture, and fatigue*. Pearsons Education, 2012.

[19] K.N Shivakumar and I.S Raju. *Treatment of singularities in cracked bodies*. Tech. rep. National Aeronautics and Space Administration, 1989.

[20] Hongjun Yu and Mainhard Kuna. "Interaction integral method for computation of crack parameters K–T – A review". In: *Engineering Fracture Mechanics* (2021).

[21] Shuai Luan, Chunguo Zhang, and Waidong Lu. "Effect of Crack Closure-Dependent Residual Stress onFatigue Crack Growth of Welded Joints Pertinent to Applied Minimum Stress Intensity". In: *Fatigue Fracture of Engineering Materials Structures* 49 (4 2026), pp. 1251–1262. DOI: https://doi.org/10.1111/ffe.70186.

[22] J. Maierhofer, R. Pippan, and H.-P. Gänser. "Modified NASGRO equation for physically short cracks". In: *International Journal of Fatigue* 59 (2013), pp. 200–207. DOI: https://doi.org/10.1016/j.ijfatigue.2013.08.019.

[23] A. Gupta, W. Sun, and C.J. Bennett. "Simulation of fatigue small crack growth in additive manufactured Ti–6Al–4V material". In: *Continuum Mechanics and Thermodynamics* 32 (2020), pp. 1745–1761. DOI: https://doi.org/10.1007/s00161-020-00878-0.

[24] J.C. Newman Jr. "A crack opening stress equation for fatigue crack growth". In: *International Journal of Fracture* 24 (1984), R131–R135. DOI: https://doi.org/10.1007/BF00020751.

[25] Morris Satin et al. "Transition modelling of surface flaws to through cracks". In: *Fatigue Fracture of Engineering Materials Structures* 43 (7 2020), pp. 1353–1367. DOI: https://doi.org/10.1111/ffe.13190.

[26] Southwest Research Institute. *Appendix D - Crack Transition Analysis, Appendix of NASGRO User's Manual*. 2025.

[27] A. Marques et al. "Multi-material Inconel 718 – Aluminium parts targeting aerospace applications: A suitable combination of low-weight and thermal properties". In: *Optics Laser Technology* 158 (2023). DOI: https://doi.org/10.1016/j.optlastec.2022.108913.

[28] Southwest Research Institute. *Appendix C - Stress Intensity Factor Formulations, Appendix of NASGRO User's Manual*. 2025.

[29] ANSYS. *Mechanical APDL 2024 R2 - Command Reference*. Version 2024 R2. URL: https://ansyshelp.ansys.com/public/account/secured?returnurl=/Views/Secured/corp/v242/en/ans_cmd/Hlp_C_CmdTOC.html.

A

Appendix A - SIF calculations in NASGRO

This appendix provides the detailed formulations for the SIF calculations implemented in NASGRO for the crack configurations considered in this thesis. These formulations are based on weight-function approaches and reference solutions as described in [28].

A.1 Semi-elliptical surface crack (SC30)

For the SC30 configuration, the applied loading is interpreted as a univariant stress distribution. Consequently, a weight-function approach is employed, where the applied stress field is multiplied by the appropriate weight function and integrated over the crack dimensions [28]:

$$K_{a,c} = \int_0^{a,c} W_{a,c}\sigma(x)dx \tag{A.1}$$

The weight function for the respective tips are defined as:

$$W_a = \frac{2}{\sqrt{2\pi(a-c)}}\left[1 + M_{1a}\sqrt{\frac{a-x}{a}} + M_{2a}\frac{a-x}{a} + M_{3a}\left(\frac{a-x}{a}\right)^{3/2}\right] \tag{A.2}$$

$$W_c = \frac{2}{\sqrt{\pi x}}\left[1 + M_{1c}\sqrt{\frac{x}{a}} + M_{2c}\frac{x}{a} + M_{3c}\left(\frac{x}{a}\right)^{3/2}\right] \tag{A.3}$$

The coefficients $M_{i(a,c)}$ depend on geometric parameters and are obtained from reference solutions. For the reference cases on which NASGRO is based, the SIF is observed to increase when approaching the free surface and to decrease sharply at the surface itself. This surface boundary effect is expected but not yet fully understood; see Section 2.1.1. For fatigue crack growth applications, NASGRO assigns the near-surface ΔK to the crack tip and multiplies it by a crack-closure correction factor β, defined as

$$\beta = \begin{cases} 0.9 + 0.2R^2 - 0.1R^4 & \text{if } R > 0 \\ 0.9 & \text{if } R \leq 0 \end{cases} \tag{A.4}$$

A.2 Quarter-elliptical corner crack (CC09)

For the CC09 configuration, the crack geometry is described using elliptical coordinates (ξ, η), as defined by NASGRO [28] and illustrated in Figure A.1. In this formulation, $\overline{Q}_x$ and $\overline{Q}_y$ represent mirror points of Q with respect to the Cartesian axes.

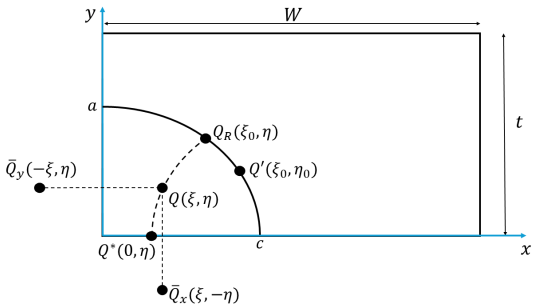

Figure A.1: Configurating and nomenclature for CC09

The applied loading is treated as a bivariant stress distribution and evaluated using a weight-function approach. The SIF is obtained by integrating over the crack surface [28]:

$$K = \int_0^a \int_0^{c\sqrt{1-y^2/a^2}} \sigma(x, y) W_{QQ'} dx dy \tag{A.5}$$

where $W_{QQ'}$ is the weighting effect on any point Q' along the crack front contributed by a point unit load applied at Q on the crack surface. The weight function depends on the crack tip location and is defined for the crack tips a and c as

$$\begin{aligned} W_{QQ^{a,c}} = \frac{\sqrt{R^2 - r^2}}{\pi l_{QQ^{a,c}}^2 \sqrt{\pi R}} \left(1 + \frac{l_{QQ^{a,c}}^2}{l_{\overline{Q}_x Q^{a,c}}^2} + \frac{l_{QQ^{a,c}}^2}{l_{\overline{Q}_y Q^{a,c}}^2}\right) \times \\ \times \left[1 + \Pi_1^{a,c} \sqrt{1 - \frac{r}{R}} + \Pi_2^{a,c} \left(1 - \frac{y}{y'}\right) + \Pi_3^{a,c} \left(1 - \frac{x}{x'}\right)\right] \end{aligned} \tag{A.6}$$

The parameters Π_1, Π_2 and Π_3 are calibrated by the reference solutions. R is the distance between Q^* and Q_R, r the distance between Q and Q^*, and $l_{QQ^{a,c}}$ represents the distance between the points Q and $Q^{a,c}$. The mirror-point distances $l_{\overline{Q}_{x,y} Q^{a,c}}$ account for free-surface effects by assuming symmetry corresponding to crack extension into the remaining quadrants.

Near-surface effects for corner cracks are not yet fully resolved within this formulation. Therefore, to remain conservative, NASGRO does not apply the crack-closure correction factor β to near-surface ΔK values for the CC09 configuration [28].

A.3 Part-elliptical through crack (TC45)

The recently introduced TC45 crack case also employs a weight-function formulation to accommodate a bivariant stress distribution. The formulation is based on the CC09 weight-function model [28]; see Section A.2. The weighting contribution at a crack-front point Q', or specifically for the crack tip points $Q^{a,c}$, resulting from a unit load applied at point Q on the crack surface, is given by

$$W_{QQ^{a,c}} = \frac{\sqrt{R^2 - r^2}}{\pi \ell^2_{QQ^{a,c}} \sqrt{\pi R}} \left(1 + \frac{\ell^2_{QQ^{a,c}}}{\ell_{Q^2_{\overline{x}Q^{a,c}}}} + \frac{\ell^2_{QQ^{a,c}}}{\ell_{Q^2_{\overline{y}Q^{a,c}}}} + \frac{\ell^2_{QQ^{a,c}}}{\ell^2_{Q_tQ^{a,c}}} + \frac{\ell^2_{QQ^{a,c}}}{\ell^2_{Q_{t\overline{x}}Q^{a,c}}} + \frac{\ell^2_{QQ^{a,c}}}{\ell^2_{Q_{t\overline{x}}Q^{a,c}}} \right) \times \\ \times \left[1 + \Pi_1 \sqrt{1 - \frac{r}{R}} + \Pi_2 \left(1 - \frac{y}{y'} \right) + \Pi_3 \left(1 - \frac{x}{x'} \right) \right] \tag{A.7}$$

The coefficients Π_i are obtained from reference solutions. The elliptical radii R and r define the locations of the points Q_R and Q, respectively, while x' and y' correspond to the position at which the unit load is applied.

The mirror points $Q_{\overline{x}}$ and $Q_{\overline{y}}$ are defined with respect to the Cartesian axes, while Q_t is mirrored with respect to the plane $y = t$. Further mirror points $Q_{t\overline{x}}$ and $Q_{t\overline{y}}$ are defined accordingly. This configuration is illustrated in Figure A.2, where Q and Q' represent points on the actual crack geometry.

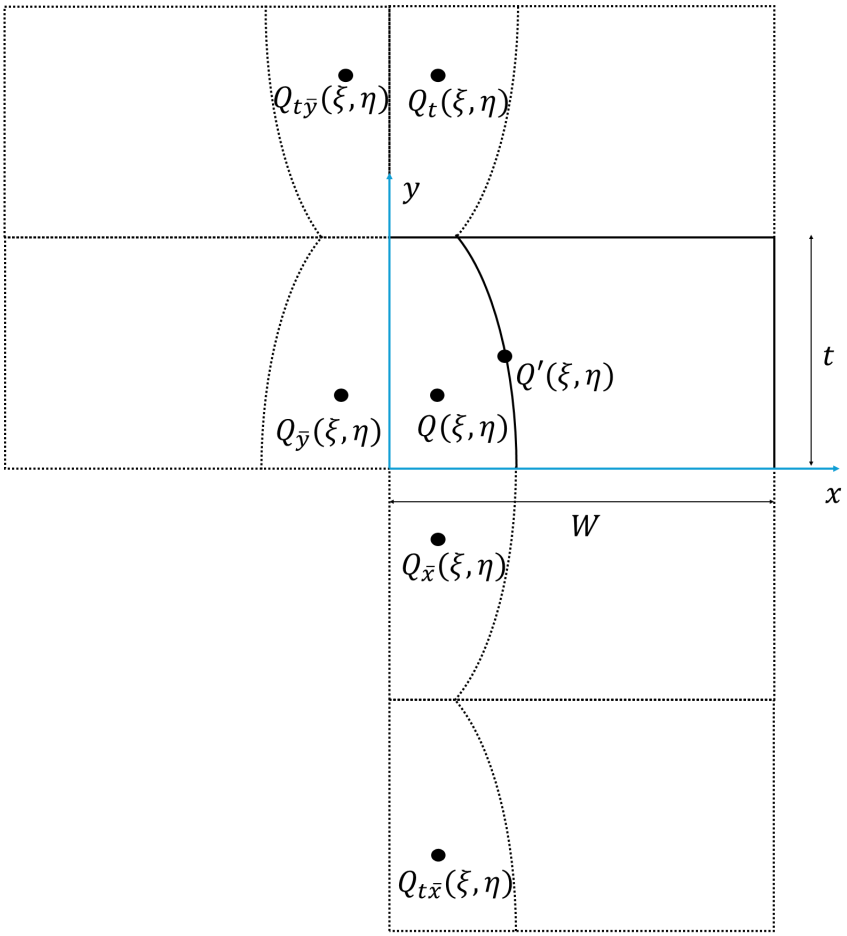

Figure A.2: Configuration and nomenclature for the TC45 crack case

To reduce computational effort, TC45 employs a patch discretisation of the crack surface. Each patch is represented by a four-node element with coordinates $[(i,j),(i+1,j),(i,j+1),(i+1,j+1)]$, and the stress field within a patch is assumed to vary linearly [28]:

$$\sigma_{i,j}^{patch} = \sum_{m=i}^{i+1} \sum_{n=j}^{j+1} f_{mn}\sigma_{mn} \tag{A.8}$$

The contribution of each corner node to the SIF is represented by $\Delta_{m,n}^{\text{patch}}$, obtained by integrating over the patch area:

$$\Delta_{m,n}^{patch} = \int_{\eta_j}^{\eta_{j+1}} \int_{\xi_i}^{\xi_{i+1}} f_{mn} W_{QQ^{a,c}}(\xi,\eta) d\xi d\eta \tag{A.9}$$

The final SIF is then computed efficiently by summing the contributions from all patches over the crack surface:

$$K = \sum_{\text{patches}} \sum_{m,n} \sigma_{mn} \Delta_{m,n}^{patch} \tag{A.10}$$

A.4 Quarter-elliptical corner crack in lug (CC19)

The CC19 configuration assumes a univariate stress distribution over the crack plane, and the SIFs are therefore evaluated using a weight function approach [28]. The model also allows for the analysis of two symmetric corner cracks within the structure; however, this capability is not explored further in this thesis.

The weight functions at the respective crack tips are defined as

$$W_c = \frac{2}{\sqrt{2\pi(c-x)}} \left[1 + M_{1c} \sqrt{\frac{c-x}{c}} + M_{2c} \frac{c-x}{c} + M_{3c} \left(\frac{c-x}{c} \right)^{3/2} \right] \tag{A.11}$$

$$W_a = \frac{2}{\sqrt{\pi x}} \left[1 + M_{1a} \sqrt{\frac{x}{c}} + M_{2a} \frac{x}{c} + M_{3a} \left(\frac{x}{c} \right)^{3/2} \right] \tag{A.12}$$

where x is the distance normal to the hole axis, measured from the location where the crack initiates. The coefficients $M_{i(a,c)}$ depend on the geometry and are obtained from reference solutions.

The SIFs at the respective crack tips are determined by integration according to

$$K_{a,c} = \int_0^c W_{a,c} \sigma(x) dx \tag{A.13}$$

where $\sigma(x)$ represents the univariate stress distribution over the crack surface.

The effect of the near free-surface constraint is, by default, accounted for in NASGRO by applying the crack-closure correction factor β to near-surface ΔK values for the CC19 configuration [28].

B

Appendix B - APDL commands

This appendix provides the APDL commands used in ANSYS to define the cyclic loading and the methods for calculating the SIFs.

B.1 NPLOAD methods

These commands are defined within the SMART crack growth module in the ANSYS file tree. They specify the methods used to evaluate the effective SIF range and the crack growth direction. Further details on these commands can be found in the ANSYS command reference manual [29].

```
! define mode-seperating method for effective SIF calculation
CGROW,NPLOAD,METH,DKMOD
! max. load method for crack growth direction
CGROW,NPLOAD,DIRECTION,KMAX
! max. tangential stress criterion for equivalent SIF
CGROW,SOPT,KEQV
```

B.2 Cyclic loading definition

These commands are defined within the Static Structural module in the ANSYS file tree and are used to define cyclic loading conditions. In addition, the region where the load is applied must be specified through a named selection. In this case, the selection *sel_tensile* refers to the surface on which a pressure load is applied. Further details on the commands can be found in the ANSYS command reference manual [29].

```
! cyclic loading definition
CLOAD,DEFINE,BEGIN
! define cyclic load table
*DIM,_cycload,TABLE,3
CLOAD,DEFINE,END

! time steps for cyclic load
_cycload(1,0) = 0
_cycload(2,0) = 0.5
_cycload(3,0) = 1
```

```
! load values (in this case pressure) for cyclic load
_cycload(1,1) = -300
_cycload(2,1) = 300
_cycload(3,1) = -300

! apply the cyclic load to a named selection
cmsel,s,sel_tensile
SF,all,pres,%_cycload%
ALLSEL,ALL

CLOAD,OUTR

! define number of cycles (not equivalent to fatigue cycles)
CLOAD,CYCNUM,1000
! define cycle period (must match the load table)
CLOAD,CYCTIME,1

CLOAD,TSTEP
```

DEPARTMENT OF MECHANICS AND MARITIME SCIENCES
CHALMERS UNIVERSITY OF TECHNOLOGY
Gothenburg, Sweden
www.chalmers.se

CHALMERS
UNIVERSITY OF TECHNOLOGY